FRONTIERS OF PHYSICS

TOPICAL REVIEW
Volume 18 / Issue 1 / 13602 / 2023

Magnetic anisotropy, exchange coupling and Dzyaloshinskii–Moriya interaction of two-dimensional magnets

Qirui Cui[1], Liming Wang[1], Yingmei Zhu[1], Jinghua Liang[1], Hongxin Yang[1,2,3,†]

1 Ningbo Institute of Materials Technology and Engineering, Chinese Academy of Sciences, Ningbo 315201, China
2 School of Physics, Nanjing University, Nanjing 210093, China
3 Center of Materials Science and Optoeledctronics Engineering, University of Chinese Academy of Sciences, Beijing 100049, China
Corresponding author. E-mail: †hongxin.yang@nimte.ac.cn
Received September 5, 2022; accepted October 11, 2022

ABSTRACT

The two-dimensional (2D) magnets provide novel opportunities for understanding magnetism and investigating spin related phenomena in several atomic thickness. Multiple features of 2D magnets, such as critical temperatures, magnetoelectric/magneto-optic responses, and spin configurations, depend on the basic magnetic terms that describe various spins interactions and cooperatively determine the spin Hamiltonian of studied systems. In this review, we present a comprehensive survey of three types of basic terms, including magnetic anisotropy that is intimately related with long-range magnetic order, exchange coupling that normally dominates the spin interactions, and Dzyaloshinskii–Moriya interaction (DMI) that favors the noncollinear spin configurations, from the theoretical aspect. We introduce not only the physical features and origin of these crucial terms in 2D magnets but also many correlated phenomena, which may lead to the advance of 2D spintronics.

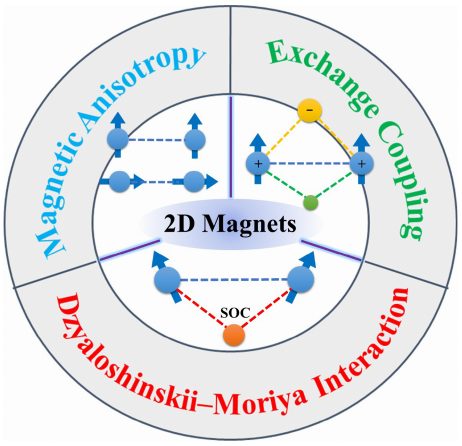

Keywords magnetic anisotropy, exchange coupling, Dzyaloshinskii–Moriya interaction, two-dimensional magnets

Contents

1 Introduction

In 1966, using Bogoliubov's inequality, Mermin and

Higher Education Press

https://doi.org/10.1007/s11467-022-1217-7

Wanger rigorously proved that both long-range ferromagnetic (FM) and antiferromagnetic (AFM) order are prohibited in a 2D isotropic Heisenberg model at finite temperatures [1]. The exciting breakthrough happens in 2017 that Huang *et al.* [3] and Gong *et al.* [2] discover the long-range ferromagnetic order in 2D van der Waals (vdW) crystals, CrI_3 and $CrGeTe_3$, with magneto-optic Kerr microscopy respectively. CrI_3 monolayer is an Ising ferromagnet with Curie temperature (T_c) of 45 K, and $CrGeTe_3$ bilayer is a Heisenberg ferromagnet with T_c of 30 K. It is believed that magnetic anisotropy removes the restriction of Merin–Wanger rules. Specifically, magnetic anisotropy opens up a spin-wave excitation gap, which is necessary for occurrence of long-range FM order at finite temperature. After the discovery of CrI_3 and $CrGeTe_3$, more and more 2D magnets with higher T_c are discovered, such as VSe_2, $MnSe_2$ and Fe_3GeTe_2 monolayers [4–6]. Besides FM systems, long-range AFM order is also observed in atomically thin crystals of $FePS_3$ and $MnPS_3$ [7, 8]. Recently, the 2D-XY magnet with in-plane rotational symmetry is realized in $CrCl_3$ monolayer on graphene/6H-SiC(001), which demonstrates that the long-range magnetism can survive in two-dimension without easy axial anisotropy [9]. Advantages of 2D magnets, such as miniaturization, flexibility, gate tunability, and high interface quality, can be further inherited by electronics devices harnessing them. The intrinsic magnetism in two dimension opens the door and further provides intensive opportunities for investigating new physical phenomena/applications of spintronics in atomic thickness. For example, the recorded tunneling magnetoresistance of 19000% is achieved in vdW magnetic tunnel junctions constructed by CrI_3 multilayers [10]; the magnetization of 2D Fe_3GeTe_2 can be effectively switched by spin–orbits torques arising from flowing current in adjacent heavy metal layer [11]; by fabricating vdW heterostructure (HS), 2D magnets could give proximity effects to 2D non-magnetic materials, which leads to the emergence of non-trivial, spin-dependent transport behavior of electrons, such as quantum anomalous Hall effects, anomalous valley Hall effect and nonlinear helical edge states [12–17]; and various topological spin configurations, including skyrmion/antiskyrmion, bimeron, vortex/antivortex, could originate from the cooperation of different magnetic parameters and appear in 2D magnets [18, 19].

All above-mentioned physical properties are closely hinged on the basic magnetic terms, which describe various spin interactions and cooperatively determine the spin Hamiltonian of studied systems. Figure 1 shows the schematics of three crucial terms, i.e., magnetic anisotropy [Fig. 1(a)], exchange interaction [Fig. 1(b)] and DMI [Fig. 1(c)], describing the preferred magnetization direction, symmetric exchange coupling, and antisymmetric exchange coupling respectively. In this review, we first introduce the magnetic anisotropy of 2D magnets.

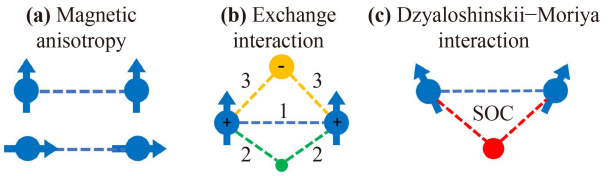

Fig. 1 The schematics of (a) magnetic anisotropy, (b) exchange interaction, and (c) Dzyaloshinskii–Moriya interaction in two-dimensional magnets. **(a)** When spins are aligned parallelly, there is always a preferred orientation of spin vectors, which is referred as the magnetic anisotropy. **(b)** Exchange coupling between two spins arises from electrons' antisymmetric wave function and can be classified as direct (blue dashed line) and indirect (green and yellow dashed lines) types. The indirect exchange couplings can be established through connecting anion (green balls) or itinerant electrons (yellow balls). **(c)** For magnets lacking inversion symmetry, Dzyaloshinskii–Moriya interaction is allowed between neighboring spin sites, which favors the noncollinear spin configurations. The spin tilting is due to the spin–orbit scattering of the nonmagnetic electrons from the mediated site (the red ball). Left and middle panel is produced from Ref. [39].

We focus on its physical relationship with magnetic order and physical origin of perpendicular magnetic anisotropy (PMA) of some well-known 2D magnets. Next, we discuss about the exchange interactions of 2D magnets, including both bilinear and high order exchange coupling. In this section, we introduce not only the definition and physical origin of these exchange coupling but also their crucial roles in determining ground or excited states of 2D magnets. Then, we introduce the DMI in 2D magnets from two aspects which are unique physical features and role in stabilizing topological quasiparticles. Finally, we summarize the contents of this review and challenges that are urgent to be solved in this flied.

2 Magnetic anisotropy of 2D magnets

2.1 Magnetic anisotropy and long-range magnetic order

The magnetic anisotropy of materials defines the preferred direction of magnetization. Figure 2(a) shows the influence of magnetic anisotropy on magnon density of states in 2D and 3D magnets. For a 2D monolayer without magnetic anisotropy, there is no spin wave excitation gap. Based on spin-wave theory, the gapless magnon will cause magnetic order collapsed in one- and two-dimensional systems. However, the magnetic anisotropy give rise the non-zero excitation gap [see Fig. 2(a)], which results in stability of long-range magnetic order at finite temperature. For multilayer system, magnon density of states (DOS) exhibit the step function of energy, and for bulk system, magnon DOS is proportional to the root of energy. Therefore, when thickness of the

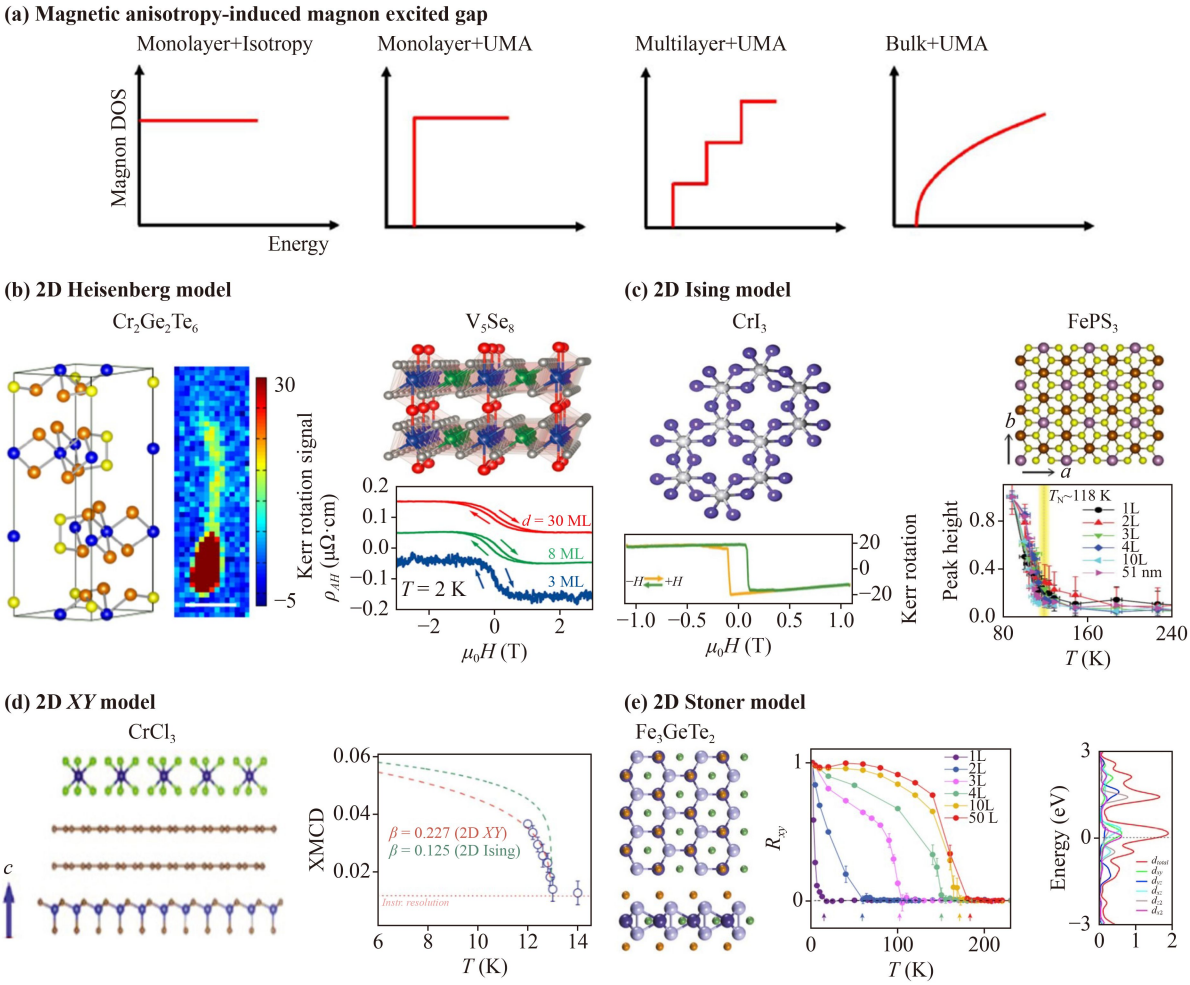

Fig. 2 **(a)** Schematics of magnetic anisotropy induced magnon excitation gap for an isotropic Heisenberg model. (b–e) Four most-widely applied models for describing the two-dimensional magnetism. **(b)** Heisenberg model: The spin vector can be along any directions in 3D space. This model is applied for describing ferromagnetism in 2D magnets with weak magnetic anisotropy, such as $Cr_2Ge_2Te_6$ (left panel) and V_5Se_8 (right panel). **(c)** Ising model: The spin is either up or down along a given direction. This model is applied for describing magnetism in 2D magnets with strong magnetic anisotropy, such as CrI_3 (left panel) and $FePS_3$ (right panel). **(d)** 2D *XY* model: The spin is constrained in the *XY* plane due to the in-plane magnetic anisotropy. $CrCl_3$ monolayer grown on Graphene/6H-SiC (0001) has been demonstrated as a 2D *XY* magnet. **(e)** Stoner model: Magnets exhibit the metallic feature and ferromagnetic order can be described by Stoner criteria. Stoner model is applied for describing magnetism in Fe_3GeTe_2 which even possesses the room-temperature ferromagnetism under ionic doping (left and middle panels). The left panel is the density of states of Fe_3GeTe_2 applied for calculating the Stoner criteria. (a) is produced from Ref. [39]. (b) is produced from Refs. [2, 20]. (c) is produced from Refs. [3, 7]. (d) is produced from Ref. [9]. (e) is produced from Refs. [6, 29].

material keeps increasing, higher temperature is required to ensure enough excitation for destroying magnetic order. Above theory has been successfully used in explaining the origin of long-range magnetic order in some 2D magnets with PMA such as $CrGeTe_3$ [2], V_5Se_8 [20], CrI_3 [3], and $FePS_3$ [7].

Ferromagnetism in $CrGeTe_3$ is observed by scanning magneto-optic Kerr microscopy [see left panel Fig. 2(b)] and well described by the isotropic Heisenberg model including perpendicular magnetic anisotropy [2]. In this model, the spin vector is allowed to rotate in three-dimensional space and thus can be written as (S_x, S_y, S_z). V_5Se_8 thin films also possess characteristics of Heisenberg-type 2D ferromagnetism as shown in right panel of Fig. 2(b) [20]. Notably, anomalous Hall effect and X-ray magnetic circular dichroism are applied for measuring the magnetism signals in V_5Se_8. Compared with $CrGeTe_3$, ferromagnetism in CrI_3 is also observed by the magneto-optic Kerr microscopy [see left panel of Fig. 2(c)] but described by the Ising model [3]. For Ising systems, the spin only has two possible states, spin "up" and spin "down". The hysteresis loops of CrI_3 layers with the external field perpendicular and parallel to sample demonstrates the existence of strong PMA. Besides ferromagnetism, Ising-type antiferromagnetism has been observed in atomically thin $FePS_3$ [see right

panel of Fig. 2(c)] by Raman spectrum [7].

Despite it is well known that PMA could stabilize 2D magnetism by lifting the limitations from thermal fluctuation [21–23], recent experiments show that it is not the essential condition for the emergence of long-range magnetic order. Magnets possess an easy plane rather than magnetic anisotropy can be described by the XY model. For a 2D XY magnet, the magnetic order can be stabilized under a finite-size limit, and the Berezinsky-Kosterlitz-Thouless (BKT) transition occurs at a critical temperature [24–28]. Using X-ray magnetic dichroism, Pinto *et al.* [9] observed that the in-plane magnetism in $CrCl_3$ monolayer grown on Graphene/6H-SiC(0001) exhibits a critical scaling behavior feature of a 2D-XY system as shown in the Fig. 2(d). The left panel and middle panel of Fig. 2(e) show the crystal structure and temperature-dependent magnetization of Fe_3GeTe_2. T_c of pristine Fe_3GeTe_2 monolayer is around 65 K [6]. Similar to bulk, Fe_3GeTe_2 monolayer remains metallic [see right panel of Fig. 2(e)]. The metallic character and non-integral magnetic moment imply that stoner model should be applied for understanding the origin magnetism [29]. For Fe_3GeTe_2 monolayer, the stoner criterion is larger than 1, thus satisfying the condition of emergence of itinerant ferromagnetic order.

For precisely obtaining the magnitudes of magnetic anisotropy, the first-principles calculations based on the density functional theory (DFT) are employed. The magnetic anisotropy energy can be obtained by comparing the energy difference between the system with in-plane and out-of-plane magnetization. Notably, strong PMA of 1.60 and 1.56 meV/unit cell is reported in CrI_3 and Fe_3GeTe_2 monolayers respectively [29–33]. With a spin Hamiltonian such as: $H = -\sum_{\langle i,j\rangle} J_{ij}(S_i \cdot S_j) - \sum_i A(S_i^z)^2$ where J and A represents the magnitude of exchange coupling and PMA, one can obtain the energy dispersion of magnon by performing the Holstein-Primakoff transformation of spin operators [34]. The first-principles calculations show that compared with $CrCl_3$ monolayer, the magnetic anisotropy of $CrWCl_6$ monolayer is significantly enhanced from in-plane –0.08 meV/unit cell to out-of-plane 2.14 meV/unit cell [35]. Therefore, the energy gap ($E_{gap} = -2AS$, A and S represents magnetic anisotropy and total spin quantum number) emerges at Γ point and the optical branch is shifted to the much higher energy level in the resolved magnon spectrum, which responds for larger enhancement of T_c. Notably, PMA-induced energy gap of magnon spectrum is also reported in the $MnBi_2Te_4$ monolayer [36].

2.2 Perpendicular magnetic anisotropy in 2D magnets

Next, we discuss about the physical origin of PMA in some well-known 2D magnets. For CrI_3 monolayer, the DFT Hamiltonian can be defined as: $H_{DFT} = H_0 + \alpha_I H_I^{soc} + \alpha_{Cr} H_{Cr}^{soc}$ where H_0 and H^{soc} represents the non-relativistic and relativistic terms respectively [30]. The magnetic anisotropy energy is dominantly contributed by non-magnetic I atom. This interesting result is further confirmed by the second-order perturbation theory [32]. Specifically, the dominant contribution to PMA of CrI_3 monolayer comes from the hybridization between occupied spin-up p_x and unoccupied spin-up p_y states of I atom. The strength of spin-orbit coupling of $5p$ orbitals in I is much stronger than that of $3d$ orbitals in Cr. Similar feature is also reported in $CrGeTe_3$ cmonolayer where the dominant contribution to PMA comes from Te atom [37]. Above scenario clearly shows that magnetic anisotropy could be modulated by electronic states of outsides non-magnetic atoms with strong SOC. By tuning interlayer distance of vdW HS, graphene/NiI_2, the PMA of NiI_2 increases over 100% [38]. This enhancement also arises from the variation of electronic states of I. Meanwhile, it is believed that in $CrGeTe_3$ monolayer, spin transition of $3d$ orbitals play crucial role in determining magnetic anisotropy [39]. Spin-conserving (-converting) transition between conduction and valence bands contributes negative magnetic (positive) anisotropy energy. DFT results show that by increasing U_{eff} of Cr to lower the energy level of majority spin in valence bands, the spin-conserving transition is largely weakened, resulting in that magnetic anisotropy energy of Cr is tuned from –100 to 200 μeV. For metallic Fe_3GeTe_2, strong PMA is intimately related with the electronic states of Fermi surface. Thus, the magnetic of anisotropy of Fe_3GeTe_2 can be effectively modulated by electron/hole doping due to the Fermi level shifting [40, 41]. Moreover, the manipulation of perpendicular magnetization of 2D magnets via electrical approaches shows the promising for the future spintronic devices. We note that the field-free perpendicular magnetization switching of Fe_3GeTe_2 is already achieved under the assistance of orbit-transfer torque in WTe_2/Fe_3GeTe_2 heterostructure [42]. By measuring the magnetization as a function of magnetic field, Seo *et al.* [43] found that PMA of $(Fe_{1-x}Co_x)_4GeTe_2$ could be tuned to be IMA when the content of Co increases. Room-temperature PMA reaching to 4.89×10^5 erg/cm^3 is confirmed in few-layer $CrTe_2$ by superconducting quantum interference device [44]. Interestingly, strong PMA is even experimentally observed in 2D magnets with layered metal–organic frameworks, where ligand-to-metal charge transfer gives rise that of anisotropy of magnetic atom [45].

3 Exchange coupling of 2D magnets

3.1 Bilinear exchange coupling

Now, we discuss about the exchange coupling between two spins that arises from electrons' antisymmetric wave function. Bilinear exchange coupling can be simply written

as: $J_{ij}(S_i \cdot S_j)$, where J_{ij} represents exchange coupling strength. Since $S_i \cdot S_j = S_{ix}S_{jx} + S_{iy}S_{jy} + S_{iz}S_{jz}$, $J_{ij}(S_i \cdot S_j)$ only describes the system with isotropic and diagonal exchange coupling terms. The bilinear exchange coupling can be further defined as: $S_i \cdot J \cdot S_j$, where J represents a 3×3 matrix containing not only diagonal but off-diagonal symmetric terms. This matrix is written as

$$J = \begin{pmatrix} J_{xx} & J_{xy} & J_{xz} \\ J_{xy} & J_{yy} & J_{yz} \\ J_{xz} & J_{yz} & J_{zz} \end{pmatrix}. \quad (1)$$

Normally, off-diagonal terms are much smaller compared with diagonal terms. By diagonalizing the matrix J, one can obtain its eigenvalues. The exchange terms in spin Hamiltonian thus could be rewritten according to these eigenvalues and specific crystal structures. When off-diagonal terms in Eq. (1) cannot be neglected, there could be sizable Kitaev interactions [46, 47]. Notably, strong Kitaev interaction that characterizes the anisotropic contribution to exchange coupling emerges in 2D magnets with magnetic atom arranging in honeycomb lattice, such as $CrGeTe_3$ and $RuCl_3$ monolayers [37, 48–58]. Moreover, it is rigorously proved that the ground state of the 2D Kitaev model of honeycomb lattice is quantum spin liquid with Majorana fermion excitations [46, 47, 59]. Such states are hopefully applied in quantum computing. For extracting magnitudes of exchange coupling, energy mapping method is the most widely used calculation algorithm [60]. All terms in J matrix [Eq. (1)] could be easily obtained by comparing the energy difference of supercells with various spin configurations.

According to the Goodenough-Kanamori-Anderson (GKA) rules [61–63], the superexchange coupling between two nearest-neighboring (NN) magnetic cations through intervening nonmagnetic anion is FM when the bonding angle of metal–ligand–metal is close to 90°. On the contrary, the direct exchange coupling between two NN magnetic cation is AFM. The competition between indirect FM and direct AFM couplings decides the final magnetic arrangement. Importantly, two conditions must be satisfied if above analysis works for 2D magnets. The first one is that octahedral crystals enforce d orbitals split into t_{2g} orbitals with low energy level and e_g orbitals with high energy level; and the second one is that d orbitals are partly occupied. The left panel of Fig. 3(a) shows the schematic of exchange coupling between two Cr atoms in CrI_3 monolayer [64]. The $e_g \leftrightarrow p \leftrightarrow t_{2g}$ superexchange allows FM coupling where the energy difference between p and d orbitals is defined as the virtual exchange gap [see right panel of Fig. 3(a)]. By engineering the d orbitals splitting to lower this gap, the energy barrier of electron hopping in the superexchange process is consequently reduced, thus resulting the significant enhancement of ferromagnetism [see Fig. 3(d)]. For magnetic atom with high spin configuration ($S = 5/2$), indirect exchange coupling should be weakly AFM [65–67]. Interestingly, intralayer ferromagnetism of $MnBi_2Te_4$ contradicts to GKA rules due to the strong hybridization between empty p orbitals of Bi and bridging Te atom [68].

Under tetrahedral crystal field, d orbitals split into e orbitals with low energy level and t_2 orbitals with low energy level. Tight-binding model shows that $e \leftrightarrow p \leftrightarrow t_2$ superexchange prefers FM coupling, however, the $e \leftrightarrow e$ and $t_2 \leftrightarrow t_2$ direct exchanges prefer AFM coupling, and the strength of $e \leftrightarrow e$ is much less than that of $t_2 \leftrightarrow t_2$ [69]. This situation is quite similar with GKA rules where $e_g \leftrightarrow p \leftrightarrow t_{2g}$ superexchange and $e_g \leftrightarrow e_g/t_{2g} \leftrightarrow t_{2g}$ direct exchange prefers FM and AFM coupling respectively. It is expected that strong AFM exchange coupling emerges when $3d$ orbitals are no less than half-filled, otherwise, strong FM coupling is achieved. This result has been further demonstrated in various 2D magnets with $p\bar{4}m2$ crystal symmetry [70]. Obviously, both direct and indirect exchange coupling between magnetic atoms is intimately related with electron occupation of outside orbitals. Therefore, different ground states could emerge under various U_{eff} that describes the electronic correlation effects. One interesting example is $Hf_2VC_2F_2$ MXene. As U_{eff} of V increases from 0 to 4 eV, $Hf_2VC_2F_2$ MXene is tuned from metal without magnetism to semiconductor with 120° noncollinear AFM ground state [71]. This noncollinear magnetism state arises from the spin frustration effect that is later observed in NiI_2 monolayer [see Fig. 3(b)]. The first-principles calculations show that the NN J_1 reaches to 7.0 meV favoring FM coupling while the third-nearest-neighboring (TNN) J_3 reaches to –5.8 meV favoring AFM coupling [72]. The cooperation of spin frustration and anisotropy of short-range symmetric exchange coupling stabilize the triangular lattice of antibiskyrmions appear in NiI_2 monolayer [see Monte Carlo simulations-obtained spin textures in Fig. 3(e)]. By applying the generalized Bloch theorem, the energy of spin system can be calculated as the function of spin spiral vector [73]. Notably, the minimized energy does not appear at Γ point rather than one position in $\Gamma - M$ direction, corresponding to noncollinear spin states. Importantly, spin helical states in $Hf_2VC_2F_2$ or NiI_2 could generate electrical polarization that is perpendicular to the helical plane, which is called as type-II multiferroics [74–76]. The ferroelectric polarization could arise from different mechanisms such as spin current and inverse DMI. Very recently, electrical polarization [see Fig. 3(f)] and chiral magnetic ground state in NiI_2 monolayer has been detected by birefringence and second-harmonic-generation measurements and circular dichroic Raman measurements, which confirms the existence of multiferroelectricity [77].

Besides the bilinear exchange coupling between

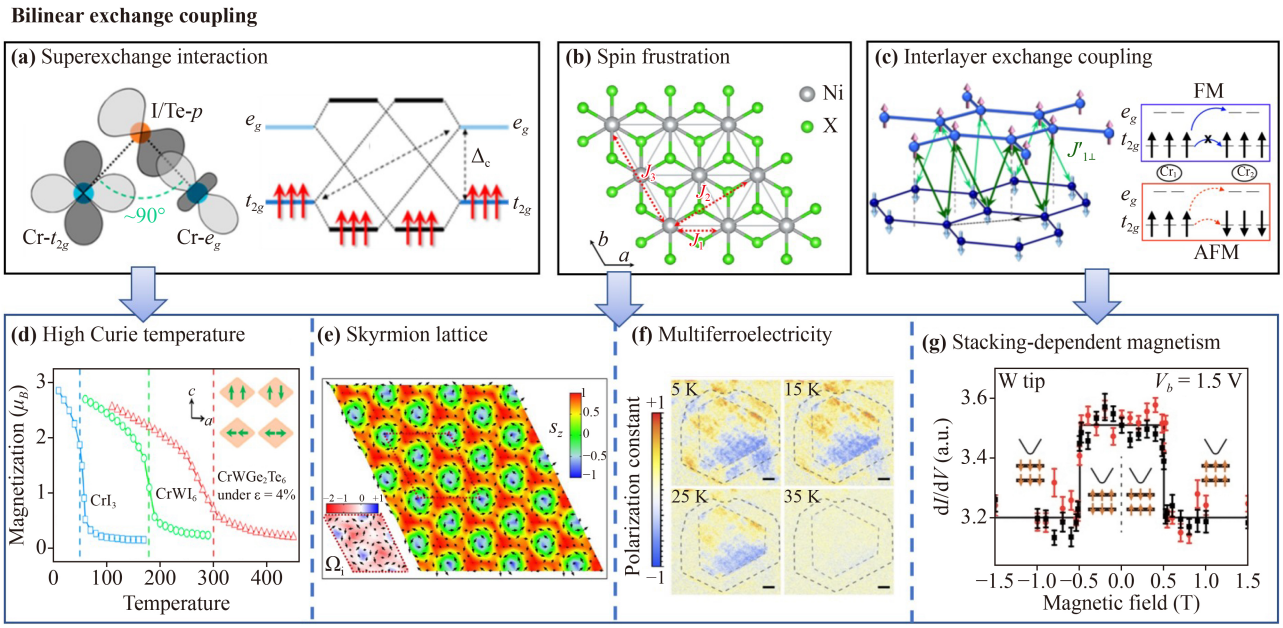

Fig. 3 Bilinear exchange coupling in 2D magnets. **(a)** Ferromagnetism in 2D magnets with octahedral crystal field, such as CrI_3, normally arises from the indirect exchange coupling. Via tuning energy splitting between t_{2g} and e_g orbitals to decrease the electron hopping barrier, the FM exchange coupling could be obviously enhanced resulting in the enhancement of Curie temperature as shown in **(d)**. **(b)** Some 2D magnets, such as NiI_2 monolayer, possess strong spin frustration that the first-neighboring and second (third)-neighboring exchange coupling has the similar magnitude but opposite sign. Spin frustration could give rise the noncollinear spin configurations as shown in **(e)**. **(f)** Moreover, the ferroelectricity probably originates from the specific noncollinear spin configurations, which thus makes system possess multiferroelectricity. **(c)** For vdW magnets, the bilinear exchange coupling also emerges between magnetic atoms in different layers, in other word, determining the interlayer magnetism. **(g)** Therefore, changing stacking configurations to modulate electron hopping path can results in the interlayer ferromagnetism-antiferromagnetism phases transition. The phenomena have been observed in CrI_3 and $CrBr_3$ bilayers by the spin polarized STM. (a) is produced from Ref. [64]. (b, d) is produced from Ref. [73]. (c) is produced from Ref. [86]. (e) is produced from Ref. [72]. (f) is produced from Ref. [77]. (g) is produced from Ref. [88].

intralayer magnetic atoms, interlayer exchange coupling also plays crucial role in determining magnetic properties of 2D magnets. For example, interlayer exchange coupling of CrI_3 bilayer can be transferred from AFM to FM states by applying bias voltage or external magnetic field [10, 78–84]. Based on the first-principles calculations and tight binding model, Xu *et al.* [85] elucidated that the AFM-to-FM phase transition arises from the electric field-induced energy splitting between electronic states of the top and bottom layers. The interlayer magnetism also intimately correlated with the stacking configurations [86–91]. Using first-principles calculations, Sivadas *et al.* [86] showed that FM interlayer exchange coupling in bilayer CrI_3 with AB stacking (low-temperature phase) could be tuned to be AFM in bi-CrI_3 with AB′ stacking (high-temperature phase). They propose that interlayer exchange coupling is dominated by super-super-exchange through Cr-I-I-Cr, and the stacking variation influences the interlayer exchange paths and numbers between two Cr atoms [see Fig. 3(c)]. As shown in Fig. 3(g), the stacking-dependent interlayer magnetism is further demonstrated in bi-$CrBr_3$ by spin-polarized scanning tunneling microscopy [88]. Moreover, Wang *et al.* [92, 93] reported the interlayer distance-dependent magnetism in MX_2 (M = V, Cr, Mn; X = S, Se, Te) bilayer where the exchange coupling is determined by the spin alignment of interlayer region. For bilayer with shorter interlayer distance, Pauli repulsion favors antiparallel arranged spins leading to interlayer AFM coupling, while for bilayer longer distance, Pauli repulsion is balanced by the kinetic-energy gain thus leading to interlayer FM coupling [92].

3.2 High-order exchange coupling

The high-order exchange coupling, such as biquadratic interaction, also plays crucial roles in determining magnetic properties of 2D magnets. In a non-Heisenberg spin Hamiltonian:

$$H = -\sum_{\langle i,j\rangle} J_{ij}\,(\boldsymbol{S}_i\cdot\boldsymbol{S}_j) - \sum_i A(S_i^z)^2 - \sum_{\langle i,j\rangle} K_{ij}(\boldsymbol{S}_i\cdot\boldsymbol{S}_j)^2, \quad (2)$$

where J_{ij} represents bilinear exchange coupling, A represents magnetic anisotropy and K_{ij} represents biquadratic exchange interaction [94, 95]. This high-order interactions arises from two electrons hopping

between different magnetic atoms as shown in Figs. 4(a) and (b) [96]. Specifically, there are two electrons hopping between spin sites with $3d$ valence electrons, and the corresponding biquadratic exchange is mediated by non-magnetic atoms with p valence electrons [see Fig. 4(b)]. By rotating spin orientation, the total energy can be written as: $E = -JS^2\cos\theta - KS^2\cos^2\theta - E_0$, where θ represents the angle between two spin vectors. Then, the explicit value K of biquadratic exchange interaction is determined by fitting energy dispersion of θ [96]. Figure 4(e) shows the normalized magnetization versus temperature T for CrI_3 monolayer whose K reaches 0.21 meV. One can see that a higher T_c is expected when K is considered in Monte Carlo simulations. Moreover, by comparing with experimental data [3], it is proved that non-Heisenberg model gives a better description of temperature-dependent magnetism. Furthermore, DMI is considered in spin Hamiltonian as

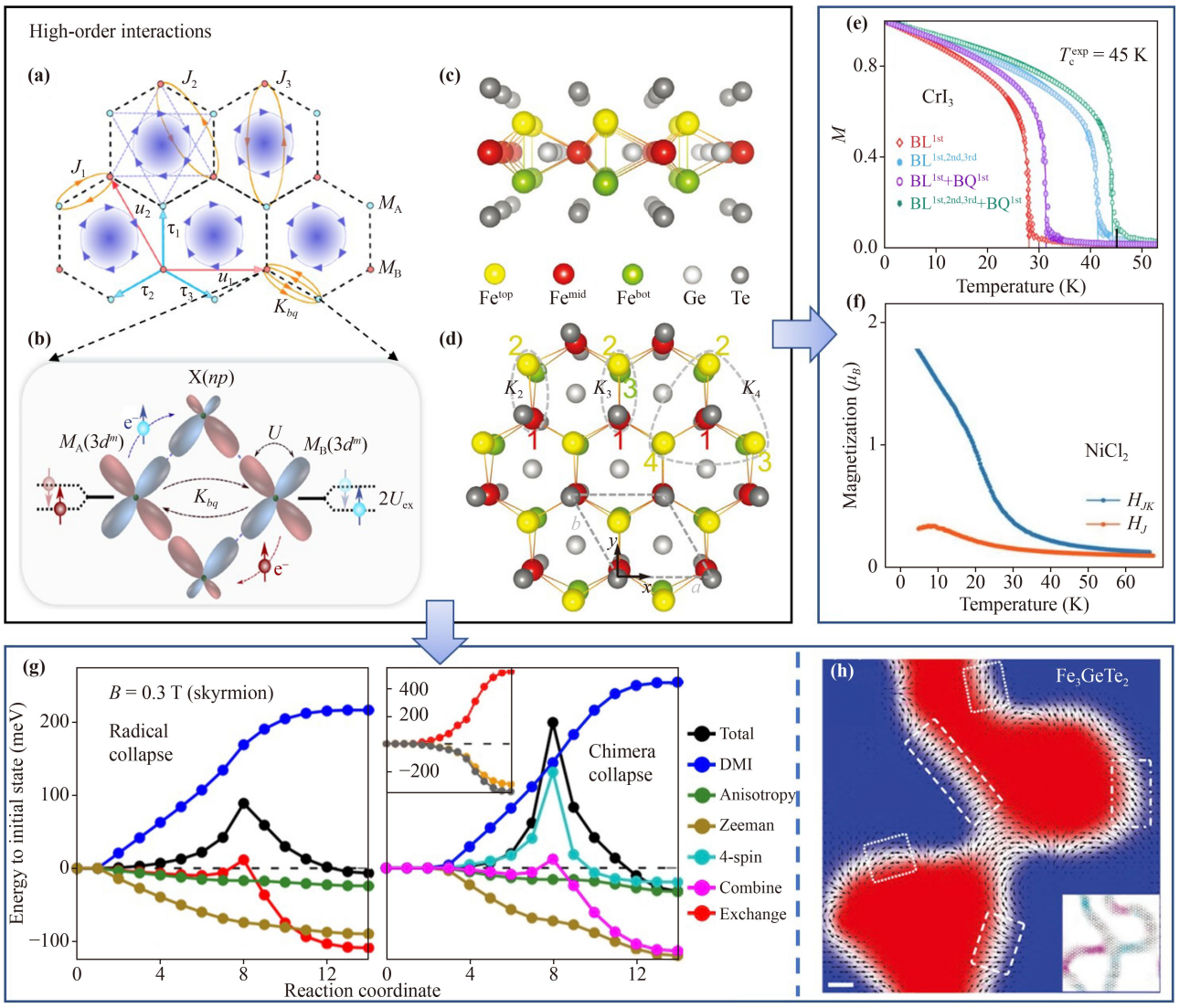

Fig. 4 High-order exchange coupling indicates that the superexchange process through the non-magnetic atom and the Coulomb repulsion at neighboring spin-sites involving more than one electron. **(a, b)** Biquadratic exchange coupling, which is also called as two-body fourth order interactions, belongs to two involving two electrons hopping between M_A and M_B sites. **(c, d)** Besides two-body fourth order interactions, three-body and four-body fourth order interactions also play crucial roles in determine magnetic features of materials such as Fe_3GeTe_2 monolayer. **(e)** Sizable biquadratic exchange coupling could favor the collinear spin configurations. For CrI_3 monolayer, the model without considering the biquadratic underestimate the Curie temperature. **(f)** Monte Carlo simulations show that in $NiCl_2$ monolayer, strong biquadratic exchange coupling transform the spin spiral ground state into the uniform ferromagnetic state. **(g)** Four-body fourth order effectively increase the energy barrier of skyrmion collapse, thus favoring the formation of non-collinear magnetism. **(h)** The high-order interactions, including two-body, three-body, and four-body interactions, play crucial roles in stabilizing topological magnetism in Fe_3GeTe_2 monolayer. (a, b, e) are produced from Ref. [96]. (c, d, h) are produced from Ref. [105]. (f) is produced from Ref. [73]. (g) is produced from Ref. [102].

$$H = -\sum_{\langle i,j\rangle} J_{ij}\,(\boldsymbol{S}_i\cdot\boldsymbol{S}_j) - \sum_i A(S_i^z)^2 - \sum_{\langle i,j\rangle} K_{ij}(\boldsymbol{S}_i\cdot\boldsymbol{S}_j)^2 - \sum_{\langle i,j\rangle} D_{ij}\cdot(\boldsymbol{S}_i\times\boldsymbol{S}_j)\,, \quad (3)$$

where D_{ij} represents the DMI vector between spin site i (S_i) and j (S_i). Despite the NN DMI vanishes due to inversion symmetry, the next-nearest-neighboring (NNN) DMI is non-negligible as inversion symmetry breaking. Using Holstein–Primakoff transformations [34], magnon dispersions are calculated based on Eq. (3). Notably, spin Hamiltonian containing biquadratic exchange interaction and DMI captures entirely most profiles of magnon dispersions measured by inelastic neutron scattering [97, 98]. Moreover, Wahab *et al.* [99] revealed that chiral domain wall with hybrid characteristic of Neel and Bloch types could arise from the cooperation of magnetic interactions shown in Eq. (3) and quantum rescaling effects. In all NiX_2 (X = Cl, Br, I) monolayers [see Fig. 3(b)], NN and TNN J have opposite signs, implying that NN and TNN J favors FM and AFM order respectively. However, spin frustration-induced nonlinear magnetism is only observed in $NiBr_2$ and NiI_2, and ground state of $NiCl_2$ turns to be linear ferromagnetism [100, 101]. Ni *et al.* [73] applied the machine learning methods to construct spin Hamiltonian and find that $NiCl_2$ possesses giant K (~0.54 meV). $NiCl_2$ clearly exhibits linear FM behavior rather than noncollinear magnetism as K is included in spin Hamiltonian [see Fig. 4(f)].

Besides enhancing ferromagnetism, high-order interaction could play crucial roles in stabilizing noncollinear spin configurations. We next introduce other high-order terms into spin Hamiltonian as

$$H = -\sum_{\langle i,j\rangle} J_{ij}\,(\boldsymbol{S}_i\cdot\boldsymbol{S}_j) - \sum_i A(S_i^z)^2 - \sum_{\langle i,j\rangle} K_{ij}(\boldsymbol{S}_i\cdot\boldsymbol{S}_j)^2 - \sum_{\langle i,j,k\rangle} Y_{ijk}(\boldsymbol{S}_i\cdot\boldsymbol{S}_j)(\boldsymbol{S}_j\cdot\boldsymbol{S}_k) - \sum_{\langle i,j,k,l\rangle} T_{ijkl}(\boldsymbol{S}_i\cdot\boldsymbol{S}_j)(\boldsymbol{S}_k\cdot\boldsymbol{S}_l) - \sum_{\langle i,j\rangle} \boldsymbol{D}_{ij}\cdot(\boldsymbol{S}_i\times\boldsymbol{S}_j)\,, \quad (4)$$

where Y_{ijk} and T_{ijkl} represents the amplitude of three-site and four-site four spin interactions respectively. In transition metal multilayers, four-site four spin interaction enhance the energy barrier [see Fig. 4(g)], thus avoiding the collapse of skyrmion/antiskyrmion into the FM state [102]. Interestingly, both Neel- and Bloch-type skyrmions are observed experimentally in Fe_3GeTe_2 multilayers although the DMI is prohibited due to inversion symmetry [103, 104]. Figure 4(c) shows the side view of Fe_3GeTe_2 where different types of Fe atom are detailly labeled [105]. Xu *et al.* [105] elucidated all possible fourth-order interactions of Fe_3GeTe_2 [see dashed circles of Fig. 4(d)] and demonstrate that Neel-, Bloch- and mixed-type chiral spin configurations can be stabilized in pristine Fe_3GeTe_2 monolayer [see Fig. 4(h)] when these interactions are considered in spin Hamiltonian.

There could be intensive interaction terms between various spin sites in real magnets besides bilinear and high-order exchange coupling, which makes calculation of these terms very complicated and time-consuming. For solving this challenge, Li *et al.* [106] proposed a machine learning approach combined with first-principles calculations to generate the realistic Hamiltonian which includes all important interaction terms in realistic materials. Furthermore, Yu *et al.* [107] proposed that an artificial neural network and a local spin descriptor could be applied to construct appropriate spin Hamiltonian for any magnets, even for magnets with topological ground states.

4 DMI of 2D magnets

4.1 Microscopic origin of DMI

As a fundamental magnetic parameter, DMI, also known as antisymmetric exchange coupling, has gained intensive attention in the last two decades due to its critical role in formation of magnetic skyrmions. In 1958, Dzyaloshinskii [108] first proposed this interaction to explain the origin of weak ferromagnetism in some AFM crystals, such as α-Fe_2O_3, $MnCO_3$, and $CoCO_3$. Specifically, an asymmetric term should be included in the free energy of these AFM crystals and is written as: $E_{DMI} = D_{ij}\cdot(\boldsymbol{S}_i\times\boldsymbol{S}_j)$. Contrary to the Heisenberg exchange coupling arranging spin collinearly, DMI drives spin to be perpendicular to each other. The competition between these two interactions finally results in tilting of spin from the collinear direction and generating the weak ferromagnetism in AFM crystals. In 1960, by extending Anderson's superexchange interaction theory, Moriya [109, 110] further proved that DMI arises from the joint effects of superexchange between spins and SOC in magnetic insulator with inversion symmetry breaking. He also gave the specific relationship between DMI vector and crystal symmetry termed as Moriya rules. In 1980, Fert and Levy elucidated that in CuMn spin-glass alloy, DMI between two magnetic atoms arises from the spin–orbit scattering of conduction electrons by nonmagnetic impurities [111, 112]. The resultant DM vector is read as

$$\boldsymbol{D}_{ijl}\left(\boldsymbol{R}_{li},\boldsymbol{R}_{lj},\boldsymbol{R}_{ij}\right) = -V_1\frac{\sin\left[k_F\left(|\boldsymbol{R}_{li}|+|\boldsymbol{R}_{lj}|+|\boldsymbol{R}_{ij}|\right)+(\pi/10)\,Z_d\right]\left(\boldsymbol{R}_{li}\cdot\boldsymbol{R}_{lj}\right)\left(\boldsymbol{R}_{li}\times\boldsymbol{R}_{lj}\right)}{|\boldsymbol{R}_{li}|^3|\boldsymbol{R}_{lj}|^3\,|\boldsymbol{R}_{ij}|}, \quad (5)$$

where $\boldsymbol{R}_{li}$, $\boldsymbol{R}_{lj}$ and $\boldsymbol{R}_{ij}$ are the corresponding distance vectors between magnetic atoms and nonmagnetic impurities, and V_1 is a SOC-governed material parameter and proportional to the SOC strength of impurity d orbitals. One can see that in Fert-Levy model, DMI depends on the relative positions of magnetic atoms and nonmagnetic impurities, and significant DMI is expected when impurities possess strong SOC. In 2015, Zhang *et al.* [113] proposed that DMI mediated by spin-polarized conduction electrons could arise from Rashba SOC termed as Rashba-type DMI.

4.2 DMI-induced topological quasiparticles

The DMI plays crucial role in stabilizing various types of topological quasiparticles in real space like skyrmion, skyrmionium, and bimeron [114]. Due to possessing multiple advantages including miniaturization, stable morphology, and current tunability, etc., magnetic skyrmions are promising for applications in the next-generation spintronic devices with high density and low-energy consumption. The earliest discovery of skyrmion is in the non-centrosymmetric B20 crystals such as MnSi [115], FeCoSi [116] and FeGe [117]. In the past decades, many efforts have been devoted to achieving strong DMI in ferromagnetic metal/heavy metal multilayers which can host room-temperature topological magnetism [118–121]. By combining cobalt and 2D materials (graphene/boron nitride) to fabricate HS, Rashba-type DMI is achieved at the interface due to potential gradient [122–125]. Recently, the 2D magnets arise intensive attention due to their appealing physical properties, and they hopefully replace the traditional bulk magnets or magnetic multilayers and lead to the development of ultracompact spintronic devices. Interestingly, both experimental and theoretical works have demonstrated that sizeable DMI and topological magnetism can be realized in 2D magnets and their HSs. Liang *et al.* [126] showed that very large DMI is achieved in Janus 2D magnets without inversion symmetry [see left panel of Fig. 5(a)]. They found that isotropic DMI of MnSeTe and MnSTe monolayers [see orange arrows in left panel of Fig. 5(a)] reaches to 2.14 and 2.63 meV, respectively [126]. These values are even comparable to those state-of-the-art ferromagnetic metal/heavy metal HSs, such as CoPt [120] and FeIr [127, 128]. The Monte Carlo simulations further elucidate that due to the competition of DMI, FM exchange coupling and magnetic anisotropy, chiral domain wall appears in MnSeTe and MnSTe and is further turned into Néel-type skyrmion particles via applying external magnetic field [see right panel of Fig. 5(a)]. Notably, isotropic DMI and it-favored various types of topological magnetism has also been predicted in many stable 2D Janus magnets, such as Cr(I, X)$_3$ (X = Cl, Br), CrTeX (X = S, Se), CrGe(Se,Te)$_3$, 1T-VXY ($X \neq Y$; X, Y = S, Se, Te), $MnBi_2(Se, Te)_4$, CrInX_3 (X = Te, Se), and $ACrX_2$ (A = Li, Na; X = S, Se, Te) monolayers [129–135]. Besides topological magnetism, 2D Janus magnets provides a fertile platform for realizing other intriguing spintronic phenomena, such as half-metallic electronic states, gate/strain/stacking-tunable magnetism, colossal PMA, and spontaneous valley polarization [136–141]. Notably, anisotropic DMI [see orange arrows in left panel of Fig. 5 (b)] can also be achieved in 2D magnets with $P\bar{4}m2$ symmetry like AX_2 [142] and $ACuX_2$ [143] monolayers (A = 3d transition metals, X= VI-A or VII-A elements). Right panel of Fig. 5(b) shows the antiskyrmion particles stabilized by anisotropic DMI.

One crucial task for practical application of topological spin textures is searching or developing electric method that can effectively manipulate these spin textures. Compared with traditional methods such as spin-polarized current, thermal excitation, and external magnetic field, electrical field is a much more energy-dissipationless method for controlling magnetism [144–147]. Due to integrating ferroelectricity, magnetism, and inversion symmetry breaking, multiferroic monolayer provides an ideal platform for realizing electrical field-controlled topological magnetism mediated by the DMI chirality reversal. Xu *et al.* [148] attested that the electrical field can flip the in-plane polarization of VOI_2 monolayer, resulting in the reversal of DMI vector. MC simulations further show that topological charge of the bimeron in VOI_2 monolayer is switched due to the reversal of DMI vector. Simultaneously, Liang *et al.* [149] demonstrated that out-of-plane electric polarization reversal in multiferroic monolayers such as CrN, $CuVP_2Se_6$, and $CuCrP_2Se_6$ can reverses the chirality of DMI as shown in left panel of Fig. 5(c). Accordingly, they define multiple skyrmion states based on the chirality and magnetization directions of skyrmion core [see right panel of Fig. 5(c)]. Furthermore, Shao *et al.* [150] showed that multiferroic monolayer can be built by intercalating magnetic atoms into nonmetallic transition-metal dichalcogenide bilayers [see left panel of Fig. 5(d)], which provides additional material candidates for electrical field-controlled skyrmion chirality as shown in Fig. 5(d).

VdW materials are easily stacked together to construct homo/heterostructures without considering lattice mismatch. Due to proximity effects or interfacial charge transfer, coupling 2D magnets to other nonmagnetic/magnetic vdW materials could modify their magnetic characteristics. Moreover, the inversion symmetry is naturally broken in the HSs, thus allowing the emergence of DMI. Notably, a large DMI energy of 1 mJ/m^2 is realized in in WTe_2/ Fe_3GeTe_2 HS, which leads to the formation of Neel-type skyrmion and chiral domain wall [151], and the Neel-type skyrmion and skyrmion crystal have been observed in Fe_3GeTe_2 multilayers where the oxide interface gives rise DMI as shown in Fig. 5(e) [152]. The left panel of Fig. 5(f) shows the

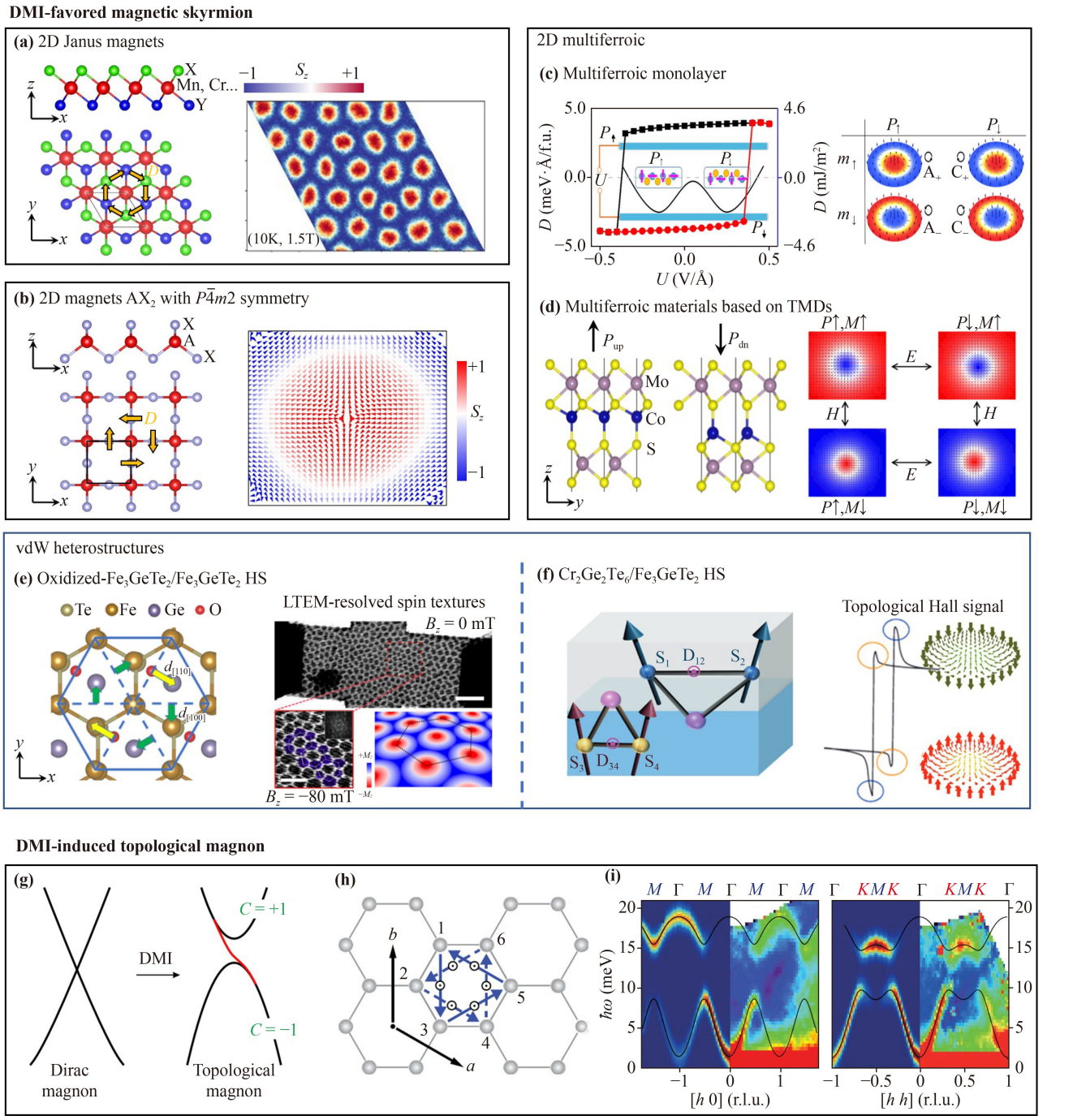

Fig. 5 DMI-induced topological quasiparticles. **(a)** The inversion symmetry breaking in 2D Janus magnets allows the isotropic DMI between neighboring spin sites as indicated by orange arrows. The Monte Carlo simulations show that topological magnetism, such as skyrmion lattice, is stabilized by the DMI. **(b)** $P\bar{4}m2$ symmetry results in the anisotropic DMI as indicated by orange arrows. This anisotropic DMI could favor the formation of novel topological quasiparticles such as antiskyrmion. The inversion symmetry breaking and electric field-controllable magnetic properties in **(c)** multiferroic monolayer and **(d)** multiferroic materials based on transition-metal dichalcogenides open the opportunities for using electric field to manipulate the topological magnetism. The skyrmion particles is experimentally observed in vdW heterostructures based on the 2D magnets, **(e)** oxidized Fe_3GeTe_2/Fe_3GeTe_2 heterostructure and **(f)** $Cr_2Ge_2Te_6$/Fe_3GeTe_2 heterostructure, by Lorenz transmission electron microscope and topological Hall effects, where noncollinear magnetism is stabilized by the interfacial DMI. **(g)** The next-neighboring DMI as indicated in **(h)** opens the non-trivial gap in magnon spectrum, which thus gives rise the topological magnon. **(i)** The non-trivial magnon gap is first observed in vdW magnets CrI_3 by neutron-scattering microscopy. (a) is produced from Ref. [126]. (b) is produced from Ref. [142]. (c) is produced from Ref. [149]. (d) is produced from Ref. [150]. (e) is produced from Ref. [152]. (g) is produced from Ref. [153]. (g) is produced from Ref. [163]. (h, i) are produced from Ref. [97].

schematic of DMI in $CrGeTe_3/Fe_3GeTe_2$ HS. Since there are two types of DMI in different FM layers, two kinds of skyrmion particles are measured by the topological Hall effects as shown in right panel of Fig. 5(f) [153].

Magnetoelectric effects in multiferroic vdW HSs constructed by 2D magnets and 2D opens novel opportunities for electrical field-controlled topological magnetism [154–159]. For example, Sun *et al.* [154] reported that the creation and annihilation of bimerons can be achieved in $LaCl/In_2Se_3$ HS by switching polarization direction of In_2Se_3. The inversion symmetry breaking of HS gives rise the in-plane DMI between La atoms, and the topological magnetism is controlled by the polarization-dependent magnetic anisotropy. Moreover, Cui *et al.* [133] proposed a kind of FE-controlled topological magnetism strategy in Janus-magnet-based multiferroic HS $MnBi_2(Se,Te)_4/In_2Se_3$. They demonstrate that various topological spin textures, including loops of vortices and antivortices and skyrmions, can be realized in this HS, and switching the direction of FE polarization of In_2Se_3 induces the transformation between different topological phases.

Besides above introduced topological spin configurations in real space, DMI can induce topological quasiparticle in reciprocal space. The magnon is a collective spin excitation in crystal lattice, which can be considered as a quantized spin wave. Topological magnon spectrum can emerges in a simple model where spin vectors arrange in the honeycomb lattice. When the spin Hamiltonian only contains Heisenberg exchange coupling, two Dirac cones appear at K and K' points in magnon spectrum [see left panel of Fig. 5(g)]. By introducing the DMI vector perpendicular to the lattice plane between the next as shown in Fig. 5(h), non-trivial magnon gap is achieved [see right panel of Fig. 5(g)] which leads to the quantized Chern number and chiral edge state [160–163]. We note that gapped magnonic topological insulating phases have been observed by inelastic neutron scattering [see Fig. 5(i)] in vdW layered magnets such as CrI_3, $CrSiTe_3$ and $CrGeTe_3$ [97, 98, 163].

5 Summary

In summary, we introduce physical features and origin of the magnetic anisotropy, exchange coupling, and DMI in 2D magnets and overview the correlated physical phenomena. Despite strong PMA favors robust ferromagnetism or antiferromagnetism, long-range magnetic order can survive in materials with "easy-plane" anisotropy. The magnetic ground state is normally dominated by spin exchange coupling that can be divided into bilinear and high-order exchange coupling. Particularly, spin frustration effects and high-order exchange coupling could generate nonlinear spin configurations, further leading to novel magnetoelectric effects. The DMI, favoring the spin spiral, have been demonstrated to be able to stabilize various topological quasiparticles in both real and reciprocal spaces. As we can see, realizing effective manipulation and cooperation of magnetic anisotropy, exchange coupling, and DMI in 2D magnets can open novel opportunities in the formation of exotic spin configurations and pave the pathway for discovery of new physics in spintronics.

Finally, it should be noted that there are still challenges in calculations of magnetic parameters in realistic materials. For explicitly obtaining values of interaction terms in spin Hamiltonian, we need to calculate the DFT energy of a supercell with different spin configurations and resolve corresponding equations. However, this method requires us to first assume important interactions in spin Hamiltonian, meaning that some crucial high-order terms or long-range interactions may not be considered. Despite significant progress have been made under the assistance of machine learning algorithm, tremendous DFT energies of supercell is necessary. Also, it is still hard to calculate spin interactions in realistic systems of large scale and/or with strongly correlation effects. Therefore, the development of novel computational approaches combining low computational cost and high accuracy is urgently expected for overcoming these problems.

6 Outlook

2D magnets provide a fertile and intriguing platform for investigating condensed matter physics [164, 165]. Since it can be easily stacked with various disimilar vdW materials, many spin-related phenomena, such as magnetoelectric/magnetoptic effects and topological/quantum matter phases, are hopefully achieved in several atomic thickness. Despite some important progress have been achieved, there are several possible research directions in future. (i) Exploring unexpected phenomena. As we mentioned before, combining 2D magnets with other vdW materials leads to the discovery of novel physicsl phenomena. However, many important matter states in real/reciprocal spaces, such as AFM skyrmion in synethic antiferromagnets and domain-controlled quantum anomalous Hall effects, have not been invesitgated in 2D magnets-based systems. (ii) Exact dynamic properties of topological magnetism in 2D magnets. It is well known that the ISB-induced DMI could stablize topological magnetism. However, the dynamic properties, such as spin-polarized current-driven motion speed and trajectory, of topological magnetism in 2D magnets are still unclear. If topological magnetism is considered as information carrier in future electronic devices, the current-driving behavior have to be clarified. (iii) Specific structures of spintronic devices. After figuring out the physical phenomena, we need to

design some protypes of spintronic devices that can make full use of advantages of 2D materials and judge its performance by comparing with traditional and commercially used devices such as STT-MTJ, which thus provides direct guidance for experimental and industrial research.

Acknowledgements This work was supported by the National Key R&D Program of China (Grant No. 2022YFA1405102), the National Natural Science Foundation of China (Grant Nos. 11874059 and 12174405), the Key Research Program of Frontier Sciences, CAS (Grant No. ZDBS-LY-7021), Ningbo Key Scientific and Technological Project (Grant No. 2021000215), "Pioneer" and "Leading Goose" R&D Program of Zhejiang Province under Grant 2022C01053, Zhejiang Provincial Natural Science Foundation (Grant No. LR19A040002), and Beijing National Laboratory for Condensed Matter Physics (Grant No. 2021000123).

References

1. N. D. Mermin and H. Wagner, Absence of ferromagnetism or antiferromagnetism in one- or two-dimensional isotropic Heisenberg models, *Phys. Rev. Lett.* 17(22), 1133 (1966)
2. C. Gong, L. Li, Z. Li, H. Ji, A. Stern, Y. Xia, T. Cao, W. Bao, C. Wang, Y. Wang, Z. Q. Qiu, R. J. Cava, S. G. Louie, J. Xia, and X. Zhang, Discovery of intrinsic ferromagnetism in two-dimensional van der Waals crystals, *Nature* 546(7657), 265 (2017)
3. B. Huang, G. Clark, E. Navarro-Moratalla, D. R. Klein, R. Cheng, K. L. Seyler, D. Zhong, E. Schmidgall, M. A. McGuire, D. H. Cobden, W. Yao, D. Xiao, P. Jarillo-Herrero, and X. Xu, Layer-dependent ferromagnetism in a van der Waals crystal down to the monolayer limit, *Nature* 546(7657), 270 (2017)
4. M. Bonilla, S. Kolekar, Y. Ma, H. C. Diaz, V. Kalappattil, R. Das, T. Eggers, H. R. Gutierrez, M. H. Phan, and M. Batzill, Strong room-temperature ferromagnetism in VSe_2 monolayers on van der Waals substrates, *Nat. Nanotechnol.* 13(4), 289 (2018)
5. D. J. O'Hara, T. Zhu, A. H. Trout, A. S. Ahmed, Y. K. Luo, C. H. Lee, M. R. Brenner, S. Rajan, J. A. Gupta, D. W. McComb, and R. K. Kawakami, Room temperature intrinsic ferromagnetism in epitaxial manganese selenide films in the monolayer limit, *Nano Lett.* 18(5), 3125 (2018)
6. Y. Deng, Y. Yu, Y. Song, J. Zhang, N. Z. Wang, Z. Sun, Y. Yi, Y. Z. Wu, S. Wu, J. Zhu, J. Wang, X. H. Chen, and Y. Zhang, Gate-tunable room-temperature ferromagnetism in two-dimensional Fe_3GeTe_2, *Nature* 563(7729), 94 (2018)
7. J. Lee, S. Lee, J. H. Ryoo, S. Kang, T. Y. Kim, P. Kim, C. H. Park, J. G. Park, and H. Cheong, Ising-type magnetic ordering in atomically thin $FePS_3$, *Nano Lett.* 16(12), 7433 (2016)
8. G. Long, H. Henck, M. Gibertini, D. Dumcenco, Z. Wang, T. Taniguchi, K. Watanabe, E. Giannini, and A. F. Morpurgo, Persistence of magnetism in atomically thin $MnPS_3$ crystals, *Nano Lett.* 20(4), 2452 (2020)
9. A. Bedoya-Pinto, J. R. Ji, A. K. Pandeya, P. Gargiani, M. Valvidares, P. Sessi, J. M. Taylor, F. Radu, K. Chang, and S. S. P. Parkin, Intrinsic 2D-XY ferromagnetism in a van der Waals monolayer, *Science* 374(6567), 616 (2021)
10. T. Song, X. Cai, M. W. Tu, X. Zhang, B. Huang, N. P. Wilson, K. L. Seyler, L. Zhu, T. Taniguchi, K. Watanabe, M. A. McGuire, D. H. Cobden, D. Xiao, W. Yao, and X. Xu, Giant tunneling magnetoresistance in spin-filter van der Waals heterostructures, *Science* 360(6394), 1214 (2018)
11. X. Wang, J. Tang, X. Xia, C. He, J. Zhang, Y. Liu, C. Wan, C. Fang, C. Guo, W. Yang, Y. Guang, X. Zhang, H. Xu, J. Wei, M. Liao, X. Lu, J. Feng, X. Li, Y. Peng, H. Wei, R. Yang, D. Shi, X. Zhang, Z. Han, Z. Zhang, G. Zhang, G. Yu, and X. Han, Current-driven magnetization switching in a van der Waals ferromagnet Fe_3GeTe_2, *Sci. Adv.* 5(8), eaaw8904 (2019)
12. H. Fu, C. Liu, and B. Yan, Exchange bias and quantum anomalous Hall effect in the $MnBi_2Te_4/CrI_3$ heterostructure, *Sci. Adv.* 6(10), eaaz0948 (2020)
13. Y. Li, J. Li, Y. Li, M. Ye, F. Zheng, Z. Zhang, J. Fu, W. Duan, and Y. Xu, High-temperature quantum anomalous Hall insulators in lithium-decorated iron-based superconductor materials, *Phys. Rev. Lett.* 125(8), 086401 (2020)
14. D. Zhong, K. L. Seyler, X. Linpeng, R. Cheng, N. Sivadas, B. Huang, E. Schmidgall, T. Taniguchi, K. Watanabe, M. A. McGuire, W. Yao, D. Xiao, K. M. C. Fu, and X. Xu, Van der Waals engineering of ferromagnetic semiconductor heterostructures for spin and valleytronics, *Sci. Adv.* 3(5), e1603113 (2017)
15. K. Zollner, P. E. Faria Junior, and J. Fabian, Proximity exchange effects in $MoSe_2$ and WSe_2 heterostructures with CrI_3: Twist angle, layer, and gate dependence, *Phys. Rev. B* 100(8), 085128 (2019)
16. L. Ai, E. Zhang, J. Yang, X. Xie, Y. Yang, Z. Jia, Y. Zhang, S. Liu, Z. Li, P. Leng, X. Cao, X. Sun, T. Zhang, X. Kou, Z. Han, F. Xiu, and S. Dong, Van der Waals ferromagnetic Josephson junctions, *Nat. Commun.* 12(1), 6580 (2021)
17. W. Zhao, Z. Fei, T. Song, H. K. Choi, T. Palomaki, B. Sun, P. Malinowski, M. A. McGuire, J. H. Chu, X. Xu, and D. H. Cobden, Magnetic proximity and nonreciprocal current switching in a monolayer WTe_2 helical edge, *Nat. Mater.* 19(5), 503 (2020)
18. Q. H. Wang, A. Bedoya-Pinto, M. Blei, A. H. Dismukes, A. Hamo, S. Jenkins, M. Koperski, Y. Liu, Q. C. Sun, E. J. Telford, H. H. Kim, M. Augustin, U. Vool, J. X. Yin, L. H. Li, A. Falin, C. R. Dean, F. Casanova, R. F. L. Evans, M. Chshiev, A. Mishchenko, C. Petrovic, R. He, L. Zhao, A. W. Tsen, B. D. Gerardot, M. Brotons-Gisbert, Z. Guguchia, X. Roy, S. Tongay, Z. Wang, M. Z. Hasan, J. Wrachtrup, A. Yacoby, A. Fert, S. Parkin, K. S. Novoselov, P. Dai, L. Balicas, and E. J. G. Santos, The magnetic genome of two-dimensional van der Waals materials, *ACS Nano* 16(5), 6960 (2022)
19. D. Soriano, M. I. Katsnelson, and J. Fernández-Rossier, Magnetic two-dimensional chromium trihalides: A theoretical perspective, *Nano Lett.* 20(9), 6225 (2020)

20. M. Nakano, Y. Wang, S. Yoshida, H. Matsuoka, Y. Majima, K. Ikeda, Y. Hirata, Y. Takeda, H. Wadati, Y. Kohama, Y. Ohigashi, M. Sakano, K. Ishizaka, and Y. Iwasa, Intrinsic 2D ferromagnetism in V_5Se_8 epitaxial thin films, *Nano Lett.* 19(12), 8806 (2019)
21. C. Tang, L. Zhang, and A. Du, Tunable magnetic anisotropy in 2D magnets via molecular adsorption, *J. Mater. Chem. C* 8(42), 14948 (2020)
22. C. Tang, K. Ostrikov, S. Sanvito, and A. Du, Prediction of room-temperature ferromagnetism and large perpendicular magnetic anisotropy in a planar hypercoordinate FeB_3 monolayer, *Nanoscale Horiz.* 6(1), 43 (2021)
23. M. Alsubaie, C. Tang, D. Wijethunge, D. Qi, and A. Du, First-principles study of the enhanced magnetic anisotropy and transition temperature in a $CrSe_2$ monolayer via hydrogenation, *ACS Appl. Electron. Mater.* 4(7), 3240 (2022)
24. V. L. Berezinskii, Destruction of long-range order in one-dimensional and two-dimensional systems having a continuous symmetry group (I): Classical systems, *Sov. Phys. JETP* 32, 493 (1971)
25. V. L. Berezinskii, Destruction of long-range order in one-dimensional and two-dimensional systems possessing a continuous symmetry group (II): Quantum systems, *Sov. Phys. JETP* 34, 610 (1972)
26. J. M. Kosterlitz and D. J. Thouless, Long range order and metastability in two dimensional solids and superfluids (application of dislocation theory), *J. Phys. C* 5(11), L124 (1972)
27. J. M. Kosterlitz and D. J. Thouless, Ordering, metastability and phase transitions in two-dimensional systems, *J. Phys. C* 6(7), 1181 (1973)
28. J. M. Kosterlitz, The critical properties of the two-dimensional *xy* model, *J. Phys. C* 7(6), 1046 (1974)
29. H. L. Zhuang, P. R. C. Kent, and R. G. Hennig, Strong anisotropy and magnetostriction in the two-dimensional Stoner ferromagnet Fe_3GeTe_2, *Phys. Rev. B* 93(13), 134407 (2016)
30. J. L. Lado and J. F. Rossier, On the origin of magnetic anisotropy in two dimensional CrI_3, *2D Mater.* 4 035002 (2017)
31. L. Webster and J. A. Yan, Strain-tunable magnetic anisotropy in monolayer $CrCl_3$, $CrBr_3$, and CrI_3, *Phys. Rev. B* 98(14), 144411 (2018)
32. B. Yang, X. Zhang, H. Yang, X. Han, and Y. Yan, Nonmetallic atoms induced magnetic anisotropy in monolayer chromium trihalides, *J. Phys. Chem. C* 123(1), 691 (2019)
33. B. Yang, X. Zhang, H. Yang, X. Han, and Y. Yan, Strain controlling transport properties of heterostructure composed of monolayer CrI_3, *Appl. Phys. Lett.* 114(19), 192405 (2019)
34. F. J. Dyson, General theory of spin-wave interactions, *Phys. Rev.* 102(5), 1217 (1956)
35. F. Xue, Y. Hou, Z. Wang, and R. Wu, Two-dimensional ferromagnetic van der Waals $CrCl_3$ monolayer with enhanced anisotropy and Curie temperature, *Phys. Rev. B* 100(22), 224429 (2019)
36. Y. Li, Z. Jiang, J. Li, S. Xu, and W. Duan, Magnetic anisotropy of the two-dimensional ferromagnetic insulator $MnBi_2Te_4$, *Phys. Rev. B* 100(13), 134438 (2019)
37. C. Xu, J. Feng, H. Xiang, and L. Bellaiche, Interplay between Kitaev interaction and single ion anisotropy in ferromagnetic CrI_3 and $CrGeTe_3$ monolayers, *npj Comput. Mater.* 4, 57 (2018)
38. Q. Cui, J. Liang, B. Yang, Z. Wang, P. Li, P. Cui, and H. Yang, Giant enhancement of perpendicular magnetic anisotropy and induced quantum anomalous Hall effect in graphene/NiI_2 heterostructures via tuning the van der Waals interlayer distance, *Phys. Rev. B* 101(21), 214439 (2020)
39. C. Gong and X. Zhang, Two-dimensional magnetic crystals and emergent heterostructure devices, *Science* 363(6428), eaav4450 (2019)
40. S. Y. Park, D. S. Kim, Y. Liu, J. Hwang, Y. Kim, W. Kim, J. Y. Kim, C. Petrovic, C. Hwang, S. K. Mo, H. Kim, B. C. Min, H. C. Koo, J. Chang, C. Jang, J. W. Choi, and H. Ryu, Controlling the magnetic anisotropy of the van der Waals ferromagnet Fe_3GeTe_2 through hole doping, *Nano Lett.* 20(1), 95 (2020)
41. Y. P. Wang, X. Y. Chen, and M. Q. Long, Modifications of magnetic anisotropy of Fe_3GeTe_2 by the electric field effect, *Appl. Phys. Lett.* 116(9), 092404 (2020)
42. X. G. Ye, P. F. Zhu, W. Z. Xu, N. Z. Shang, K. H. Liu, and Z. M. Liao, Orbit-transfer torque driven field-free switching of perpendicular magnetization chin, *Phys. Lett.* 39, 037303 (2022)
43. J. Seo, E. S. An, T. Park, S. Y. Hwang, G. Y. Kim, K. Song, W. Noh, J. Y. Kim, G. S. Choi, M. Choi, E. Oh, K. Watanabe, T. Taniguchi, J. H. Park, Y. J. Jo, H. W. Yeom, S. Y. Choi, J. H. Shim, and J. S. Kim, Tunable high-temperature itinerant antiferromagnetism in a van der Waals magnet, *Nat. Commun.* 12(1), 2844 (2021)
44. X. Zhang, Q. Lu, W. Liu, W. Niu, J. Sun, J. Cook, M. Vaninger, P. F. Miceli, D. J. Singh, S. W. Lian, T. R. Chang, X. He, J. Du, L. He, R. Zhang, G. Bian, and Y. Xu, Room-temperature intrinsic ferromagnetism in epitaxial $CrTe_2$ ultrathin films, *Nat. Commun.* 12(1), 2492 (2021)
45. Y. Wang, M. E. Ziebel, L. Sun, J. T. Gish, T. J. Pearson, X. Z. Lu, A. E. Thorarinsdottir, M. C. Hersam, J. R. Long, D. E. Freedman, J. M. Rondinelli, D. Puggioni, and T. D. Harris, Strong magnetocrystalline anisotropy arising from metal–ligand covalency in a metal–organic candidate for 2D magnetic order, *Chem. Mater.* 33(22), 8712 (2021)
46. A. Kitaev, Fault-tolerant quantum computation by anyons, *Ann. Phys.* 303(1), 2 (2003)
47. A. Kitaev, Anyons in an exactly solved model and beyond, *Ann. Phys.* 321(1), 2 (2006)
48. C. Xu, J. Feng, M. Kawamura, Y. Yamaji, Y. Nahas, S. Prokhorenko, Y. Qi, H. Xiang, and L. Bellaiche, Possible Kitaev quantum spin liquid state in 2D materials with $S = 3/2$, *Phys. Rev. Lett.* 124(8), 087205 (2020)
49. L. J. Sandilands, Y. Tian, K. W. Plumb, Y. J. Kim, and K. S. Burch, Scattering continuum and possible fractionalized excitations in α-$RuCl_3$, *Phys. Rev. Lett.* 114(14), 147201 (2015)
50. H.-S. Kim, V. Vijay Shankar, A. Catuneanu, and H. Y. Kee, Kitaev magnetism in honeycomb $RuCl_3$ with intermediate spin–orbit coupling, *Phys. Rev. B* 91,

241110(R) (2015)
51. A. Banerjee, C. A. Bridges, J. Q. Yan, A. A. Aczel, L. Li, M. B. Stone, G. E. Granroth, M. D. Lumsden, Y. Yiu, J. Knolle, S. Bhattacharjee, D. L. Kovrizhin, R. Moessner, D. A. Tennant, D. G. Mandrus, and S. E. Nagler, Proximate Kitaev quantum spin liquid behaviour in a honeycomb magnet, *Nat. Mater.* 15(7), 733 (2016)
52. S. M. Winter, Y. Li, H. O. Jeschke, and R. Valentí, Challenges in design of Kitaev materials: Magnetic interactions from competing energy scales, *Phys. Rev. B* 93(21), 214431 (2016)
53. H. S. Kim and H. Y. Kee, Crystal structure and magnetism in α-$RuCl_3$: An *ab initio* study, *Phys. Rev. B* 93(15), 155143 (2016)
54. M. Hermanns, I. Kimchi, and J. Knolle, Physics of the Kitaev model: Fractionalization, dynamic correlations, and material connections, *Annu. Rev. Condens. Matter Phys.* 9(1), 17 (2018)
55. A. Banerjee, P. Lampen-Kelley, J. Knolle, C. Balz, A. A. Aczel, B. Winn, Y. Liu, D. Pajerowski, J. Yan, C. A. Bridges, A. T. Savici, B. C. Chakoumakos, M. D. Lumsden, D. A. Tennant, R. Moessner, D. G. Mandrus, and S. E. Nagler, Excitations in the field-induced quantum spin liquid state of α-$RuCl_3$, *npj Quant. Mater.* 3, 8 (2018)
56. Y. Kasahara, K. Sugii, T. Ohnishi, M. Shimozawa, M. Yamashita, N. Kurita, H. Tanaka, J. Nasu, Y. Motome, T. Shibauchi, and Y. Matsuda, Unusual thermal Hall effect in a Kitaev spin liquid candidate α-$RuCl_3$, *Phys. Rev. Lett.* 120(21), 217205 (2018)
57. H. Takagi, T. Takayama, G. Jackeli, G. Khaliullin, and S. E. Nagler, Concept and realization of Kitaev quantum spin liquids, *Nat. Rev. Phys.* 1(4), 264 (2019)
58. J. A. Sears, L. E. Chern, S. Kim, P. J. Bereciartua, S. Francoual, Y. B. Kim, and Y. J. Kim, Ferromagnetic Kitaev interaction and the origin of large magnetic anisotropy in α-$RuCl_3$, *Nat. Phys.* 16(8), 837 (2020)
59. Y. Zhou, K. Kanoda, and T. K. Ng, Quantum spin liquid states, *Rev. Mod. Phys.* 89(2), 025003 (2017)
60. H. J. Xiang, E. J. Kan, S. H. Wei, M. H. Whangbo, and X. G. Gong, Predicting the spin-lattice order of frustrated systems from first principles, *Phys. Rev. B* 84(22), 224429 (2011)
61. B. Goodenough, Theory of the role of covalence in the perovskite-type manganites [La,M(II)] MnO_3, *Phys. Rev.* 100(2), 564 (1955)
62. J. Kanamori, Superexchange interaction and symmetry properties of electron orbitals, *J. Phys. Chem. Solids* 10(2–3), 87 (1959)
63. P. W. Anderson, New approach to the theory of superexchange interactions, *Phys. Rev.* 115(1), 2 (1959)
64. C. Huang, J. Feng, F. Wu, D. Ahmed, B. Huang, H. Xiang, K. Deng, and E. Kan, Toward intrinsic room-temperature ferromagnetism in two-dimensional semiconductors, *J. Am. Chem. Soc.* 140(36), 11519 (2018)
65. N. Sivadas, M. W. Daniels, R. H. Swendsen, S. Okamoto, and D. Xiao, Magnetic ground state of semiconducting transition-metal trichalcogenide monolayers, *Phys. Rev. B* 91(23), 235425 (2015)
66. Q. Pei and W. Mi, Electrical control of magnetic behavior and valley polarization of monolayer antiferromagnetic $MnPSe_3$ on an insulating ferroelectric substrate from first principle, *Phys. Rev. Appl.* 11(1), 014011 (2019)
67. T. Olsen, Magnetic anisotropy and exchange interactions of two-dimensional $FePS_3$, $NiPS_3$ and $MnPS_3$ from first principles calculations, *J. Phys. D* 54(31), 314001 (2021)
68. J. Li, J. Y. Ni, X. Y. Li, H. J. Koo, M. H. Whangbo, J. S. Feng, and H. J. Xiang, Intralayer ferromagnetism between $S = 5/2$ ions in $MnBi_2Te_4$: Role of empty Bi p states, *Phys. Rev. B* 101(20), 201408 (2020)
69. C. Huang, J. Feng, J. Zhou, H. Xiang, K. Deng, and E. Kan, Ultra-high-temperature ferromagnetism in intrinsic tetrahedral semiconductors, *J. Am. Chem. Soc.* 141(31), 12413 (2019)
70. Q. Cui, Y. Zhu, Y. Ga, J. Liang, P. Li, D. Yu, P. Cui, and H. Yang, Anisotropic Dzyaloshinskii–Moriya interaction and topological magnetism in two-dimensional magnets protected by $P\bar{4}m2$ crystal symmetry, *Nano Lett.* 22(6), 2334 (2022)
71. J. J. Zhang, L. Lin, Y. Zhang, M. Wu, B. I. Yakobson, and S. Dong, Type-II multiferroic $Hf_2VC_2F_2$ MXene monolayer with high transition temperature, *J. Am. Chem. Soc.* 140(30), 9768 (2018)
72. D. Amoroso, P. Barone, and S. Picozzi, Spontaneous skyrmionic lattice from anisotropic symmetric exchange in a Ni-halide monolayer, *Nat. Commun.* 11(1), 5784 (2020)
73. J. Y. Ni, X. Y. Li, D. Amoroso, X. He, J. S. Feng, E. J. Kan, S. Picozzi, and H. J. Xiang, Giant biquadratic exchange in 2D magnets and its role in stabilizing ferromagnetism of $NiCl_2$ monolayers, *Phys. Rev. Lett.* 127(24), 247204 (2021)
74. H. Katsura, N. Nagaosa, and A. V. Balatsky, Spin current and magnetoelectric effect in noncollinear magnets, *Phys. Rev. Lett.* 95(5), 057205 (2005)
75. D. Khomskii, Classifying multiferroics: Mechanisms and effects, *Physics (College Park Md.)* 2, 20 (2009)
76. Y. Tokura, S. Seki, and N. Nagaosa, Multiferroics of spin origin, *Rep. Prog. Phys.* 77(7), 076501 (2014)
77. Q. Song, C. A. Occhialini, E. Ergeçen, B. Ilyas, D. Amoroso, P. Barone, J. Kapeghian, K. Watanabe, T. Taniguchi, A. S. Botana, S. Picozzi, N. Gedik, and R. Comin, Evidence for a single-layer van der Waals multiferroic, *Nature* 602(7898), 601 (2022)
78. D. R. Klein, D. MacNeill, J. L. Lado, D. Soriano, E. Navarro-Moratalla, K. Watanabe, T. Taniguchi, S. Manni, P. Canfield, J. Fernández-Rossier, and P. Jarillo-Herrero, Probing magnetism in 2D van der Waals crystalline insulators via electron tunneling, *Science* 360(6394), 1218 (2018)
79. Z. Wang, I. Gutiérrez-Lezama, N. Ubrig, M. Kroner, M. Gibertini, T. Taniguchi, K. Watanabe, A. Imamoğlu, E. Giannini, and A. F. Morpurgo, Very large tunneling magnetoresistance in layered magnetic semiconductor CrI_3, *Nat. Commun.* 9(1), 2516 (2018)
80. H. H. Kim, B. Yang, T. Patel, F. Sfigakis, C. Li, S. Tian, H. Lei, and A. W. Tsen, One million percent tunnel magnetoresistance in a magnetic van der Waals

heterostructure, *Nano Lett.* 18(8), 4885 (2018)
81. S. Jiang, L. Li, Z. Wang, K. F. Mak, and J. Shan, Controlling magnetism in 2D CrI_3 by electrostatic doping, *Nat. Nanotechnol.* 13(7), 549 (2018)
82. S. Jiang, J. Shan, and K. F. Mak, Electric-field switching of two-dimensional van der Waals magnets, *Nat. Mater.* 17(5), 406 (2018)
83. B. Huang, G. Clark, D. R. Klein, D. MacNeill, E. Navarro-Moratalla, K. L. Seyler, N. Wilson, M. A. McGuire, D. H. Cobden, D. Xiao, W. Yao, P. Jarillo-Herrero, and X. Xu, Electrical control of 2D magnetism in bilayer CrI_3, *Nat. Nanotechnol.* 13(7), 544 (2018)
84. H. H. Kim, B. Yang, S. Li, S. Jiang, C. Jin, Z. Tao, G. Nichols, F. Sfigakis, S. Zhong, C. Li, S. Tian, D. G. Cory, G. X. Miao, J. Shan, K. F. Mak, H. Lei, K. Sun, L. Zhao, and A. W. Tsen, Evolution of interlayer and intralayer magnetism in three atomically thin chromium trihalides, *Proc. Natl. Acad. Sci. USA* 116(23), 11131 (2019)
85. R. Xu and X. Zhou, Electric field-modulated magnetic phase transition in van der Waals CrI_3 bilayers, *J. Phys. Chem. Lett.* 11(8), 3152 (2020)
86. N. Sivadas, S. Okamoto, X. Xu, C. J. Fennie, and D. Xiao, Stacking-dependent magnetism in bilayer CrI_3, *Nano Lett.* 18(12), 7658 (2018)
87. P. Jiang, C. Wang, D. Chen, Z. Zhong, Z. Yuan, Z. Y. Lu, and W. Ji, Stacking tunable interlayer magnetism in bilayer CrI_3, *Phys. Rev. B* 99(14), 144401 (2019)
88. W. Chen, Z. Sun, Z. Wang, L. Gu, X. Xu, S. Wu, and C. Gao, Direct observation of van der Waals stacking-dependent interlayer magnetism, *Science* 366(6468), 983 (2019)
89. J. Xiao and B. Yan, An electron-counting rule to determine the interlayer magnetic coupling of the van der Waals materials, *2D Mater.* 7, 045010 (2020)
90. T. Li, S. Jiang, N. Sivadas, Z. Wang, Y. Xu, D. Weber, J. E. Goldberger, K. Watanabe, T. Taniguchi, C. J. Fennie, K. Fai Mak, and J. Shan, Pressure-controlled interlayer magnetism in atomically thin CrI_3, *Nat. Mater.* 18(12), 1303 (2019)
91. Y. Xu, A. Ray, Y. T. Shao, S. Jiang, K. Lee, D. Weber, J. E. Goldberger, K. Watanabe, T. Taniguchi, D. A. Muller, K. F. Mak, and J. Shan, Coexisting ferromagnetic–antiferromagnetic state in twisted bilayer CrI_3, *Nat. Nanotechnol.* 17(2), 143 (2022)
92. C. Wang, X. Zhou, L. Zhou, Y. Pan, Z. Y. Lu, X. G. Wan, X. Q. Wang, and W. Ji, Bethe–Slater-curve-like behavior and interlayer spin-exchange coupling mechanisms in two-dimensional magnetic bilayers, *Phys. Rev. B* 102, 020402(R) (2020)
93. L. Wu, L. Zhou, X. Zhou, C. Wang, and W. Ji, In-plane epitaxy-strain-tuning intralayer and interlayer magnetic coupling in $CrSe_2$ and $CrTe_2$ monolayers and bilayers, *Phys. Rev. B* 106(8), L081401 (2022)
94. J. C. Slonczewski, Fluctuation mechanism for biquadratic exchange coupling in magnetic multilayers, *Phys. Rev. Lett.* 67(22), 3172 (1991)
95. N. S. Fedorova, C. Ederer, N. A. Spaldin, and A. Scaramucci, Biquadratic and ring exchange interactions in orthorhombic perovskite manganites, *Phys. Rev. B* 91(16), 165122 (2015)
96. A. Kartsev, M. Augustin, R. F. L. Evans, K. S. Novoselov, and E. J. G. Santos, Biquadratic exchange interactions in two-dimensional magnets, *npj Comput. Mater.* 6, 150 (2020)
97. L. Chen, J. H. Chung, B. Gao, T. Chen, M. B. Stone, A. I. Kolesnikov, Q. Huang, and P. Dai, Topological spin excitations in honeycomb ferromagnet CrI_3, *Phys. Rev. X* 8(4), 041028 (2018)
98. L. Chen, J. H. Chung, M. B. Stone, A. I. Kolesnikov, B. Winn, V. O. Garlea, D. L. Abernathy, B. Gao, M. Augustin, E. J. G. Santos, and P. Dai, Magnetic field effect on topological spin excitations in CrI_3, *Phys. Rev. X* 11(3), 031047 (2021)
99. D. A. Wahab, M. Augustin, S. M. Valero, W. Kuang, S. Jenkins, E. Coronado, I. V. Grigorieva, I. J. Vera-Marun, E. Navarro-Moratalla, R. F. L. Evans, K. S. Novoselov, and E. J. G. Santos, Quantum rescaling, domain metastability, and hybrid domain-walls in 2D CrI_3 magnets, *Adv. Mater.* 33(5), 2004138 (2021)
100. P. A. Lindgard, R. J. Birgeneau, J. Als-Nielsen, and H. J. Guggenheim, Spin-wave dispersion and sublattice magnetization in $NiCl_2$, *J. Phys. Chem.* 8, 1059 (1975)
101. Z. Jiang, Y. Li, W. Duan, and S. Zhang, Half-excitonic insulator: A single-spin Bose–Einstein condensate, *Phys. Rev. Lett.* 122(23), 236402 (2019)
102. S. Paul, S. Haldar, S. von Malottki, and S. Heinze, Role of higher-order exchange interactions for skyrmion stability, *Nat. Commun.* 11(1), 4756 (2020)
103. B. Ding, Z. Li, G. Xu, H. Li, Z. Hou, E. Liu, X. Xi, F. Xu, Y. Yao, and W. Wang, Observation of magnetic skyrmion bubbles in a van der Waals ferromagnet Fe_3GeTe_2, *Nano Lett.* 20(2), 868 (2020)
104. M. T. Birch, L. Powalla, S. Wintz, O. Hovorka, K. Litzius, J. C. Loudon, L. A. Turnbull, V. Nehruji, K. Son, C. Bubeck, T. G. Rauch, M. Weigand, E. Goering, M. Burghard, and G. Schütz, History-dependent domain and skyrmion formation in 2D van der Waals magnet Fe_3GeTe_2, *Nat. Commun.* 13(1), 3035 (2022)
105. C. Xu, X. Li, P. Chen, Y. Zhang, H. Xiang, and L. Bellaiche, Assembling diverse skyrmionic phases in Fe_3GeTe_2 monolayers, *Adv. Mater.* 34(12), 2107779 (2022)
106. X. Y. Li, F. Lou, X. G. Gong, and H. Xiang, Constructing realistic effective spin Hamiltonians with machine learning approaches, *New J. Phys.* 22(5), 053036 (2020)
107. H. Yu, C. Xu, X. Li, F. Lou, L. Bellaiche, Z. Hu, X. Gong, and H. Xiang, Complex spin Hamiltonian represented by an artificial neural network, *Phys. Rev. B* 105(17), 174422 (2022)
108. I. Dzyaloshinsky, A thermodynamic theory of "weak" ferromagnetism of antiferromagnetics, *J. Phys. Chem. Solids* 4(4), 241 (1958)
109. T. Moriya, New mechanism of anisotropic superexchange interaction, *Phys. Rev. Lett.* 4(5), 228 (1960)
110. T. Moriya, Anisotropic superexchange interaction and weak ferromagnetism, *Phys. Rev.* 120(1), 91 (1960)
111. A. Fert and P. M. Levy, Role of anisotropic exchange interactions in determining the properties of spin-glasses, *Phys. Rev. Lett.* 44(23), 1538 (1980)

112. P. M. Levy and A. Fert, Anisotropy induced by nonmagnetic impurities in Cu Mn spin-glass alloys, *Phys. Rev. B* 23(9), 4667 (1981)
113. A. Kundu and S. Zhang, Dzyaloshinskii–Moriya interaction mediated by spin-polarized band with Rashba spin–orbit coupling, *Phys. Rev. B* 92(9), 094434 (2015)
114. A. Fert, N. Reyren, and V. Cros, Magnetic skyrmions: Advances in physics and potential applications, *Nat. Rev. Mater.* 2(7), 17031 (2017)
115. S. Mühlbauer, B. Binz, F. Jonietz, C. Pfleiderer, A. Rosch, A. Neubauer, R. Georgii, and P. Böni, Skyrmion lattice in a chiral magnet, *Science* 323(5916), 915 (2009)
116. X. Yu, Y. Onose, N. Kanazawa, J. H. Park, J. H. Han, Y. Matsui, N. Nagaosa, and Y. Tokura, Real-space observation of a two-dimensional skyrmion crystal, *Nature* 465(7300), 901 (2010)
117. X. Yu, N. Kanazawa, Y. Onose, K. Kimoto, W. Z. Zhang, S. Ishiwata, Y. Matsui, and Y. Tokura, Near room-temperature formation of a skyrmion crystal in thin-films of the helimagnet FeGe, *Nat. Mater.* 10(2), 106 (2011)
118. C. Moreau-Luchaire, C. Moutafis, N. Reyren, J. Sampaio, C. A. F. Vaz, N. Van Horne, K. Bouzehouane, K. Garcia, C. Deranlot, P. Warnicke, P. Wohlhüter, J. M. George, M. Weigand, J. Raabe, V. Cros, and A. Fert, Additive interfacial chiral interaction in multilayers for stabilization of small individual skyrmions at room temperature, *Nat. Nanotechnol.* 11(5), 444 (2016)
119. A. Soumyanarayanan, M. Raju, A. L. Gonzalez Oyarce, A. K. C. Tan, M. Y. Im, A. P. Petrović, P. Ho, K. H. Khoo, M. Tran, C. K. Gan, F. Ernult, and C. Panagopoulos, Tunable room-temperature magnetic skyrmions in Ir/Fe/Co/Pt multilayers, *Nat. Mater.* 16(9), 898 (2017)
120. O. Boulle, J. Vogel, H. Yang, S. Pizzini, D. de Souza Chaves, A. Locatelli, T. O. Menteş, A. Sala, L. D. Buda-Prejbeanu, O. Klein, M. Belmeguenai, Y. Roussigné, A. Stashkevich, S. M. Chérif, L. Aballe, M. Foerster, M. Chshiev, S. Auffret, I. M. Miron, and G. Gaudin, Room-temperature chiral magnetic skyrmions in ultrathin magnetic nanostructures, *Nat. Nanotechnol.* 11(5), 449 (2016)
121. H. Yang, O. Boulle, V. Cros, A. Fert, and M. Chshiev, Controlling Dzyaloshinskii–Moriya interaction via chirality dependent atomic-layer stacking, insulator capping and electric field, *Sci. Rep.* 8(1), 12356 (2018)
122. A. Kundu and S. Zhang, Dzyaloshinskii–Moriya interaction mediated by spin-polarized band with Rashba spin-orbit coupling, *Phys. Rev. B* 92(9), 094434 (2015)
123. A. A. Ado, A. Qaiumzadeh, R. A. Duine, A. Brataas, and M. Titov, Asymmetric and symmetric exchange in a generalized 2D Rashba ferromagnet, *Phys. Rev. Lett.* 121(8), 086802 (2018)
124. H. Yang, G. Chen, A. A. C. Cotta, A. T. N'Diaye, S. A. Nikolaev, E. A. Soares, W. A. A. Macedo, K. Liu, A. K. Schmid, A. Fert, and M. Chshiev, Significant Dzyaloshinskii–Moriya interaction at graphene-ferromagnet interfaces due to the Rashba effect, *Nat. Mater.* 17(7), 605 (2018)
125. A. Hallal, J. Liang, F. Ibrahim, H. Yang, A. Fert, and M. Chshiev, Rashba-type Dzyaloshinskii–Moriya interaction, perpendicular magnetic anisotropy, and skyrmion states at 2D materials/Co interfaces, *Nano Lett.* 21(17), 7138 (2021)
126. J. Liang, W. Wang, H. Du, A. Hallal, K. Garcia, M. Chshiev, A. Fert, and H. Yang, Very large Dzyaloshinskii-Moriya interaction in two-dimensional Janus manganese dichalcogenides and its application to realize skyrmion states, *Phys. Rev. B* 101(18), 184401 (2020)
127. S. Heinze, K. von Bergmann, M. Menzel, J. Brede, A. Kubetzka, R. Wiesendanger, G. Bihlmayer, and S. Blügel, Spontaneous atomic scale magnetic skyrmion lattice in two dimensions, *Nat. Phys.* 7(9), 713 (2011)
128. A. Belabbes, G. Bihlmayer, F. Bechstedt, S. Blügel, and A. Manchon, Hund's rule-driven Dzyaloshinskii–Moriya interaction at 3d–5d interfaces, *Phys. Rev. Lett.* 117(24), 247202 (2016)
129. C. Xu, J. Feng, S. Prokhorenko, Y. Nahas, H. Xiang, and L. Bellaiche, Topological spin texture in Janus monolayers of the chromium trihalides $Cr(I,X)_3$, *Phys. Rev. B* 101(6), 060404 (2020)
130. Y. Zhang, C. Xu, P. Chen, et al., Emergence of skyrmionium in a two-dimensional $CrGe(Se,Te)_3$ Janus monolayer, *Phys. Rev. B* 102, 241107(R) (2020)
131. S. Laref, V. Goli, I. Smaili, et al., Topologically stable bimerons and skyrmions in vanadium dichalcogenide Janus monolayers, arXiv: 2011.07813 (2011)
132. J. Jiang, X. Liu, R. Li, and W. Mi, Topological spin textures in a two-dimensional $MnBi_2(Se,Te)_4$ Janus material, *Appl. Phys. Lett.* 119(7), 072401 (2021)
133. Q. Cui, Y. Zhu, J. Jiang, J. Liang, D. Yu, P. Cui, and H. Yang, Ferroelectrically controlled topological magnetic phase in a Janus-magnet-based multiferroic heterostructure, *Phys. Rev. Res.* 3(4), 043011 (2021)
134. W. Du, K. Dou, Z. He, Y. Dai, B. Huang, and Y. Ma, Spontaneous magnetic skyrmions in single-layer $CrInX_3$ (X = Te, Se), *Nano Lett.* 22(8), 3440 (2022)
135. P. Li, Q. Cui, Y. Ga, J. Liang, and H. Yang, Large Dzyaloshinskii–Moriya interaction and field-free topological chiral spin states in two-dimensional alkali-based chromium chalcogenides, *Phys. Rev. B* 106(2), 024419 (2022)
136. F. Zhang, W. Mi, and X. Wang, Spin-dependent electronic structure and magnetic anisotropy of 2D ferromagnetic Janus $Cr_2I_3X_3$ (X = Br, Cl) monolayers, *Adv. Electron. Mater.* 1900778 (2019)
137. F. Zhang, H. Zhang, W. Mi, and X. Wang, Electronic structure, magnetic anisotropy and Dzyaloshinskii–Moriya interaction in Janus $Cr_2I_3X_3$ (X = Br, Cl) bilayers, *Phys. Chem. Chem. Phys.* 22(16), 8647 (2020)
138. R. Li, J. Jiang, X. Shi, W. Mi, and H. Bai, Two-dimensional Janus FeXY (X, Y = Cl, Br, and I, $X \neq Y$) monolayers: Half-metallic ferromagnets with tunable magnetic properties under strain, *ACS Appl. Mater. Interfaces* 13(32), 38897 (2021)
139. J. Jiang, R. Li, and W. Mi, Electrical control of topological spin textures in two-dimensional multiferroics, *Nanoscale* 13(48), 20609 (2021)
140. Y. Xu, S. Qi, and W. Mi, Electronic structure and magnetic properties of two-dimensional h-BN/Janus

2H-VSeX (X = S, Te) van der Waals heterostructures, *Appl. Surf. Sci.* 537, 147898 (2021)

141. S. Qi, J. Jiang, X. Wang, and W. Mi, Valley polarization, magnetic anisotropy and Dzyaloshinskii–Moriya interaction of two-dimensional graphene/Janus 2H-VSeX (X = S, Te) heterostructures, *Carbon* 174, 540 (2021)
142. Q. Cui, Y. Zhu, Y. Ga, J. Liang, P. Li, D. Yu, P. Cui, and H. Yang, Anisotropic Dzyaloshinskii–Moriya interaction and topological magnetism in two-dimensional magnets protected by $P\bar{4}m2$ crystal symmetry, *Nano Lett.* 22(6), 2334 (2022)
143. Y. Ga, Q. Cui, Y. Zhu, D. Yu, L. Wang, J. Liang, and H. Yang, Anisotropic Dzyaloshinskii–Moriya interaction protected by D_{2d} crystal symmetry in two-dimensional ternary compounds, *npj Comput. Mater.* 8, 128 (2022)
144. F. Matsukura, Y. Tokura, and H. Ohno, Control of magnetism by electric fields, *Nat. Nanotechnol.* 10(3), 209 (2015)
145. P. J. Hsu, A. Kubetzka, A. Finco, N. Romming, K. von Bergmann, and R. Wiesendanger, Electric-field-driven switching of individual magnetic skyrmions, *Nat. Nanotechnol.* 12(2), 123 (2017)
146. C. Tang, L. Zhang, S. Sanvito, and A. Du, Electric-controlled half-metallicity in magnetic van der Waals heterobilayer, *J. Mater. Chem. C* 8(21), 7034 (2020)
147. L. Zhang, C. Tang, S. Sanvito, Y. Gu, and A. Du, Hydrogen-intercalated 2D magnetic bilayer: Controlled magnetic phase transition and half-metallicity via ferroelectric switching, *ACS Appl. Mater. Interfaces* 14(1), 1800 (2022)
148. C. Xu, P. Chen, H. Tan, Y. Yang, H. Xiang, and L. Bellaiche, Electric-field switching of magnetic topological charge in type-I multiferroics, *Phys. Rev. Lett.* 125(3), 037203 (2020)
149. J. Liang, Q. Cui, and H. Yang, Electrically switchable Rashba-type Dzyaloshinskii–Moriya interaction and skyrmion in two-dimensional magnetoelectric multiferroics, *Phys. Rev. B* 102(22), 220409 (2020)
150. Z. Shao, J. Liang, Q. Cui, M. Chshiev, A. Fert, T. Zhou, and H. Yang, Multiferroic materials based on transition-metal dichalcogenides: Potential platform for reversible control of Dzyaloshinskii–Moriya interaction and skyrmion via electric field, *Phys. Rev. B* 105(17), 174404 (2022)
151. Y. Wu, S. Zhang, J. Zhang, W. Wang, Y. L. Zhu, J. Hu, G. Yin, K. Wong, C. Fang, C. Wan, X. Han, Q. Shao, T. Taniguchi, K. Watanabe, J. Zang, Z. Mao, X. Zhang, and K. L. Wang, Néel-type skyrmion in WTe_2/Fe_3GeTe_2 van der Waals heterostructure, *Nat. Commun.* 11(1), 3860 (2020)
152. T. E. Park, L. Peng, J. Liang, A. Hallal, F. S. Yasin, X. Zhang, K. M. Song, S. J. Kim, K. Kim, M. Weigand, G. Schütz, S. Finizio, J. Raabe, K. Garcia, J. Xia, Y. Zhou, M. Ezawa, X. Liu, J. Chang, H. C. Koo, Y. D. Kim, M. Chshiev, A. Fert, H. Yang, X. Yu, and S. Woo, Néel-type skyrmions and their current-induced motion in van der Waals ferromagnet-based heterostructures, *Phys. Rev. B* 103(10), 104410 (2021)
153. Y. Wu, B. Francisco, W. Wang, et al., A van der Waals interface hosting two groups of magnetic skyrmions, a van der Waals interface hosting two groups of magnetic skyrmions, *Adv. Mater.* 34(16), 2110583 (2022)
154. W. Sun, W. Wang, H. Li, G. Zhang, D. Chen, J. Wang, and Z. Cheng, Controlling bimerons as skyrmion analogues by ferroelectric polarization in 2D van der Waals multiferroic heterostructures, *Nat. Commun.* 11(1), 5930 (2020)
155. C. K. Li, X. P. Yao, and G. Chen, Writing and deleting skyrmions with electric fields in a multiferroic heterostructure, *Phys. Rev. Res.* 3(1), L012026 (2021)
156. K. Dou, W. Du, Y. Dai, B. Huang, and Y. Ma, Two-dimensional magnetoelectric multiferroics in a MnSTe/In_2Se_3 heterobilayer with ferroelectrically controllable skyrmions, *Phys. Rev. B* 105(20), 205427 (2022)
157. W. Sun, W. Wang, J. Zang, H. Li, G. Zhang, J. Wang, and Z. Cheng, Manipulation of magnetic skyrmion in a 2D van der Waals heterostructure via both electric and magnetic fields, *Adv. Funct. Mater.* 31(47), 2104452 (2021)
158. W. Sun, W. Wang, H. Li, X. Li, Z. Yu, Y. Bai, G Zhang, and Z. Cheng, $LaBr_2$ bilayer multiferroic moiré superlattice with robust magnetoelectric coupling and magnetic bimerons, *npj Comput. Mater.* 8, 159 (2022)
159. J. Chen and S. Dong, Manipulation of magnetic domain walls by ferroelectric switching: Dynamic magnetoelectricity at the nanoscale, *Phys. Rev. Lett.* 126, 117603 (2021)
160. Y. Onose, T. Ideue, H. Katsura, Y. Shiomi, N. Nagaosa, and Y. Tokura, Observation of the magnon Hall effect, *Science* 329(5989), 297 (2010)
161. R. Matsumoto and S. Murakami, Theoretical prediction of a rotating magnon wave packet in ferromagnets, *Phys. Rev. Lett.* 106(19), 197202 (2011)
162. R. Chisnell, J. S. Helton, D. E. Freedman, D. K. Singh, R. I. Bewley, D. G. Nocera, and Y. S. Lee, Topological magnon bands in a kagome lattice ferromagnet, *Phys. Rev. Lett.* 115(14), 147201 (2015)
163. F. Zhu, L. Zhang, X. Wang, F. J. dos Santos, J. Song, T. Mueller, K. Schmalzl, W. F. Schmidt, A. Ivanov, J. T. Park, J. Xu, J. Ma, S. Lounis, S. Blügel, Y. Mokrousov, Y. Su, and T. Brückel, Topological magnon insulators in two-dimensional van der Waals ferromagnets $CrSiTe_3$ and $CrGeTe_3$: Toward intrinsic gap-tunability, *Sci. Adv.* 7(37), eabi7532 (2021)
164. X. Yu, X. Zhang, Q. Shi, S. Tian, H. Lei, K. Xu, and H. Hosono, Large magnetocaloric effect in van der Waals crystal $CrBr_3$, *Front. Phys.* 14(4), 43501 (2019)
165. Q. Pei, X. C. Wang, J. J. Zou, and W. B. Mi, Tunable electronic structure and magnetic coupling in strained two-dimensional semiconductor $MnPSe_3$, *Front. Phys.* 13(4), 137105 (2018)